OFFICE OF CIVILIAN RADIOACTIVE WASTE MANAGEMENT
CALCULATION COVER SHEET

1. QA: QA

Page: 1 Of: 28

2. Calculation Title
Breakage of Commercial Spent Nuclear Fuel Cladding by Mechanical Loading

3. Document Identifier (including Revision Number)
CAL-EBS-MD-000001 REV 00

MOL.19991213.0237

4. Total Attachments	5. Attachment Numbers - Number of pages in each
8	I-5, II-1, III-2, IV-1, V-3, VI-2, VII-1, VIII-9

6 JKM 12-3-1999

	Print Name	Signature	Date
6. Originator	J. Kevin McCoy	J Kevin McCoy	11-1-1999
7. Checker	Zekai Ceylan	Zekai Ceylan	11/2/99
8. Lead	Christine Stockman	David Stahl for Christine Stockman	12/3/99

9. Remarks
This calculation contains TBV-3480 and TBV-3481.

THE TECHNICAL CHECKER CONCURS WITH CHANGES MADE BETWEEN REV 00B AND REV 00.
ZC. 12/3/99

Revision History

10. Revision No.	11. Description of Revision
00	Initial issue.

WMIS01
MOL.19991213.0237

CONTENTS

1. PURPOSE

The purpose of this calculation is to calculate the expected rate for breakage of commercial spent nuclear fuel cladding caused by mechanical loading. This report supports the development of process modeling for waste form degradation. The associated activity in which the results will ultimately be used is performance assessment. This document was prepared in accordance with AP-3.12Q/Rev. 0/ICN 0. The development plan for this document is Ref. 27.

Referencing in this calculation refers to the document input numbers appearing in column 2a of the Document Input Reference Sheets (DIRS), Attachment VIII hereto.

2. METHOD

For seismic loading, the equations of motion for a fuel rod in an assembly are solved for impact of the assembly on an unyielding surface. The solution to the equations of motion is used to determine the fragility, that is, the probability that the fuel rod will break under the specified loading. The fragility is convolved with the seismic hazard to determine the rate of rod breakage.

For static loading by backfill or rubble, the amount of material is used to determine the gravitational load on a fuel rod. That load is compared with the load a rod can support to determine whether the rods can support the load.

3. ASSUMPTIONS

One assumption is made for this calculation: The emplaced solid materials (waste packages, drift lining, invert, drip shields, backfill, etc.) in the emplacement drift are sufficient to fill half of the drift with rubble. This assumption is used in Attachment VI. The basis for the assumption is engineering judgment concerning the amount of void space that can be practicably filled. This assumption does not require verification because, as is discussed in Section 6.2, the results do not depend on the amount of materials in the drift.

4. USE OF COMPUTER SOFTWARE AND MODELS

4.1 SOFTWARE APPROVED FOR QUALITY ASSURANCE (QA) WORK

None used.

4.2 SOFTWARE ROUTINES

Attachments I, III, V, and VI document a software routine, RODBREAK V1.0. Since this is the initial release of this routine, no change history is provided. All parts of the software routine run under Mathcad 8 Professional on a personal computer.

Inputs to Attachment I are the number of links in half of chain n and the time step $\Delta\tau$. Attachment I has been verified for n from 3 to 32, inclusive. For each value of n, there is a corresponding range of $\Delta\tau$ for which the calculation works correctly. Table 1 lists values of n and

$\Delta\tau$ for which the routine has been verified. To verify the routine on first use, use it as documented in Attachment I, with $n = 16$ and $\Delta\tau = 0.000002$. It should provide $extmcurv_{0,0} = -0.585$ and $extmcurv_{n,1} = 0.384$.

Inputs to Attachment III are three vectors, all of the same length: the distances of the joints from the support x, the minimum curvature at each joint *Cmin*, and the maximum curvature at each joint *Cmax*. The routine has been verified for the following range of input parameters. Let $n+1$ be the number of elements in each vector. For $i = 0, 1, ..., n-1$, one must have $x_i < x_{i+1}$. For $i = 0, 1, ..., n$, one must have $Cmin_i \le 0$ and $Cmax_i \ge 0$. To verify the routine on first use, use it as documented in Attachment III along with the input file `beam curvature.txt` listed in Attachment II. The routine should provide $PP_0 = 1$, $PP_8 = 0.0999$, and $PP_{15} = 7.832 \cdot 10^{-5}$.

Inputs to Attachment V are the seismic hazard curves (*loghah* vs. *pgah*, *loghav* vs. *pgav*, *loghvh* vs. *pgvh*, and *loghvv* vs. *pgvv*) and the fracture fragility curve (*Pfr* vs. *Kv*). The routine has been verified for the following range of input parameters. The vectors *loghah* and *pgah* must have the same number of elements; let this number be $n+1$. The seismic hazard curves must have $pgah_{i+1} > pgah_i$, $loghah_{i+1} < loghah_i$ for $i = 0, 1, ..., n-1$. In addition, one must have $pgah_0 > 0$. Analogous restrictions apply to the other three seismic hazard curves. *Pfr* and *Kv* must have the same number of elements; let this number be $m+1$. One must have $Kv_{j+1} > Kv_j$, $Pfr_{j+1} < Pfr_j$ for $j = 0, 1, ..., m-1$. In addition, one must have $Kv_0 = 0$ and $Pfr_0 = 1$. To verify the routine on first use, use it as documented in Attachment V along with the input file `fract_curve.txt` listed in Attachment IV. The routine should provide $vrup = 3.347$ m·s^{-1}, $(2 \cdot ahmax \cdot gap)^{1/2} = 1.266$ m·s^{-1}, and seismic risks as tabulated in Table 2.

Inputs to Attachment VI are the fractional density of rubble ψ, the fraction of the original drift cross section that is filled before collapse occurs f, and the drift radius r. The routine has been verified for $0 \le f \le 1$, $0 < \psi \le (4-\pi)/(4+\pi-2\pi f)$, and $r < 0$. (In the terms of the attachment, the upper limit on ψ assures that $h1 \ge 0$.) To verify the routine on first use, set $\psi = 0.5$ and $f = 0$. The routine should give $h1 = 1.3562$, $h2 = 2.0000$, and $h3 = 3.6034$. This result has been verified by hand calculations.

4.3 MODELS

None used.

5. CALCULATION

The results presented in this calculation are subject to TBV-3480 and TBV-3481. Qualification status of data is discussed in Section 5.1. Sections 6.1 and 6.2 explain why some data do not affect the results.

The calculation is divided into three parts. First, the inputs to the calculation are listed. Second, the effects of seismic loading are discussed. Third, the effects of static loading are discussed.

The calculation is focused on the performance of a W1717WL fuel assembly, also known as Westinghouse 17 × 17 LOPAR or Westinghouse 17 × 17 Standard assembly (Ref. 17). This fuel type has been chosen for two reasons. First, it is the most common type of pressurized water reactor fuel assembly (Ref. 16). Second, it is expected to have fairly low mechanical strength because of its thin cladding, slender rods, and large grid-to-grid spacing. Consequently, it is expected to be either representative of or more fragile than typical pressurized water reactor fuel.

5.1 INPUTS

The number of digits in the values cited herein may reflect an input from another source, an artifact of units conversion, or a recitation of computer output; consequently, the number of digits should not be interpreted as an indication of accuracy.

The following information on accepted data is used:

- Request that data "developed under Nuclear Regulatory Commission (NRC) approved Quality Assurance (QA) programs and used in facilities licensed by the NRC" (Ref. 1) should be considered as accepted data.
- Approval of the request made in Ref. 1 (Ref. 2).

Refs. 1 and 2 are used only as references to support the position that data from Ref. 11 are accepted data.

The following information on masses and densities is used:

- Molar mass of natural uranium: 238.0289 g (Ref. 3).
- Molar mass of oxygen: 15.9994 g (Ref. 3).
- Density of zirconium: 6520 kg/m^3 (Ref. 4).

The information in Refs. 3 and 4 is established fact and is therefore accepted data.

The following information on mechanical properties is used:

- Elastic modulus of irradiated Zircaloy cladding in bending at room temperature: 145.5 GPa (Ref. 5). This value is the arithmetic mean of the values 133 GPa (Ref. 5, Table 34, line 1) and 158 GPa (Ref. 5, Table 35, line 5).
- Yield strength (0.02% maximum fiber strain) of irradiated Zircaloy cladding in bending at room temperature: 1.55 GPa (Ref. 5). This value is the arithmetic mean of the values 1.57 GPa (Ref. 5, Table 34, line 1) and 1.53 GPa (Ref. 5, Table 35, line 5).
- Fracture toughness of irradiated cladding, fifth percentile value: 17 MPa·m$^{1/2}$ (Ref. 7).

The data from Ref. 5 are existing; they are subject to TBV-3480. The yield strength and elastic modulus given above are substantially larger than values for uniaxial tension tests that have been published elsewhere. The differences may reflect the biaxial stresses that are imposed during bending and the methods of data analysis used in Ref. 5. The authors of Ref. 5 applied equations for simple beams to calculate the quantities from loads and deflections; they did not measure

actual stresses and strains. Room-temperature properties are used here because seismic effects are primarily of interest for times long after emplacement, when the fuel will have cooled to approximately room temperature. The qualification status of the datum from Ref. 7 has not been determined. However, as is discussed in Section 6.1, the uncertainty in the datum from Ref. 7 does not affect the results, so the quality of this datum is immaterial.

The following information on flaws in cladding is used:

- Number of pellet-clad interaction flaws per pressurized water reactor fuel rod: 60 (Ref. 8).
- Frequency of rod failure by pellet-clad interaction: 10^{-4} (Ref. 9).
- Size of critical flaw as a fraction of cladding thickness: 0.28 (Ref. 10).

The qualification status of the data from Refs. 8, 9, and 10 has not been determined. However, as is discussed in Section 6.1, the uncertainty in the data from Refs. 8, 9, and 10 does not affect the results, so the quality of these data is immaterial.

The following information on the design of a W1717WL (Westinghouse 17 × 17 LOPAR) fuel assembly is used:

- Number of fuel rods per assembly: 264 (Ref. 11, Table 2-2).
- Rod pitch: 12.5984 mm (Ref. 11, Table 2-2).
- Width of a spacer grid: 214.0204 mm (Ref. 11, Figure 2-3).
- Active length: 3657.6 mm (Ref. 11, Figure 2-4).
- Maximum distance between two spacer grids: 620.52 mm (Ref. 11, Figure 2-4). This is the difference between the measurements 777.75 mm and 157.23 mm.
- Amount of uranium per assembly: 461.50 kg (Ref. 11, Table 3-1). The largest of the masses given in Ref. 11, Table 3-1 is used because it might be nonconservative to use a smaller mass.
- Outside diameter of cladding: 9.4996 mm (Ref. 11, Table 3-1).
- Thickness of cladding: 0.5715 mm (Ref. 11, Table 3-1). This value is half of the difference between the outside diameter (9.4996 mm) and the inside diameter (8.3566 mm) of the cladding.

Ref. 11 is simply a summary of data presented in a proprietary document that was developed under an NRC-approved quality assurance program and used in a facility licensed by the NRC. Therefore, all the data in Ref. 11 are accepted data.

The following information on waste package design is used:

- Inside width of pressurized water reactor fuel basket tube: 226.4 mm (Attachment VII).

The qualification status of the datum from Attachment VII has not been determined. However, as is discussed in Section 6.1, the uncertainty in the datum from Attachment VII does not affect the results, so the quality of this datum is immaterial.

The following information on seismic hazard is used:

- Seismic hazard for horizontal peak ground acceleration (Ref. 12).
- Seismic hazard for horizontal peak ground velocity (Ref. 12).
- Seismic hazard for vertical peak ground acceleration (Ref. 25).
- Seismic hazard for vertical peak ground velocity (Ref. 25).

Annual probabilities of exceedance as functions of peak ground acceleration or velocity are reported in Attachment V. The data in Ref. 12 are subject to TBV-3481.

The following information on rubble in a collapsed drift is used:

- Dry bulk density of TSw2 tuff: 2270 ± 80 kg/m^3 (Ref. 13).
- Fractional solids content (fractional density) of graded granular powder: 0.60 (Ref. 14).
- Diameter of waste emplacement drift: 5.5 m (Ref. 15).

A fractional density of 0.60 is typical of the densities listed for tight packings in Ref. 14, though that particular value is not listed. The qualification status of the data from Refs. 13, 14, and 15 has not been determined. However, as is discussed in Section 5.3.2, the uncertainty in the data from Refs. 13, 14, and 15 does not affect the results, so the quality of these data is immaterial.

The following information on fuel assembly types is used:

- Number of pressurized water reactor fuel assemblies discharged, by type (Ref. 16).
- Descriptions of fuel assembly types (Ref. 17).

Data from Ref. 16 are used only to justify the choice of W1717WL as the fuel assembly type to be considered. Refs. 16 and 17 are references only, not sources of input. Therefore, these data are not directly relied upon to address safety or waste isolation issues. The descriptions of types in Ref. 17 are used to show that (1) a Westinghouse 17 × 17 LOPAR fuel assembly, referred to in Ref. 2 by code W1717W, is in fact identical to type W1717WL and (2) the drawing in Ref. 1 is of a W1717WL fuel assembly. Since this source is used only to enhance traceability, the information from this source is not directly relied upon to address safety or waste isolation issues.

The following information on Hamiltonian mechanics is used:

- Hamilton's equations of motion (Ref. 6).

The information in Ref. 6 is established fact and is therefore accepted data. The form of Hamilton's equations is given in Section 5.2.1.

The following information on fracture mechanics is used:

- Equations for stress intensity factor for a surface crack in a tube subjected to bending loads (Ref. 18).

- Normalized stress intensity factor for a surface crack in a tube subjected to bending loads (Ref. 19).

Refs. 18 and 19 are used as references only, not as sources of input. The information in Refs. 18 and 19 is used only to show that it is conservative to use a simpler treatment. These references are discussed in Section 5.2.5.

The following information on beam theory is used:

- Equation for moment of inertia of a hollow circle (Ref. 20).
- Equation for maximum fiber stress in a simple beam (Ref. 21).
- Equation for maximum bending moment in a simple beam with left end fixed, right end fixed (Ref. 22).

The information in Refs. 20 through 22 is established fact and is therefore accepted data. These equations are given in Section 5.3.1.

The following information on series expansions is used:

- Equation for series expansion for exponential function (Ref. 23).

The information in Ref. 23 is established fact and is therefore accepted data. This expansion is given in Attachment III.

The following information on gravitation is used:

- Standard acceleration of gravity: 9.80665 m/s^2 (Ref. 24).

The information in Ref. 24 is established fact and is therefore accepted data.

5.2 SEISMIC LOADING

If an earthquake shakes an emplacement drift, the ground motion will cause vibration of fuel rods inside the waste packages. If the ground motion and vibration are sufficiently strong, the fuel rods may break. This calculation examines the motion of fuel rods and provides an estimate of the rate at which fuel rods would fail.

The expected rate for breakage of fuel rods will depend on the fragility of the rods and the seismic hazard. Fragility is the probability that a fuel rod will fail when it is exposed to loading of a given strength, and strength is some measure of ground motion, such as peak ground velocity. The seismic hazard is the frequency with which earthquakes of a given strength occur. The expected rate of failure is obtained by multiplying the fragility by the seismic hazard and summing over all strengths. Seismic hazard and risk are discussed quantitatively in Section 5.2.6. Different hazards (such as peak ground velocity and peak ground acceleration) give rise to different fragilities. It should be noted that the seismic hazard is often given slightly differently. For example, two seismic hazard curves may be seen in Ref. 26. In those figures, the annual

probability of exceedance is given as a function of the peak ground velocity. The hazard mentioned in the discussion above would be the negative of the first derivative of the curves shown in the figures.

The configuration of the fuel assemblies, waste package, and emplacement drift is quite uncertain at times long after emplacement, so it is necessary to consider limiting cases for seismic loading. Two loading scenarios are considered here. Both describe the impact of an assembly on an unyielding flat surface. In the first scenario, the assembly strikes the surface at the peak ground velocity. This could occur if a waste package is at rest in a drift, the ground moves horizontally, and the side of the drift strikes the waste package at the instant of peak ground velocity. This description is conservative in that (1) no credit is taken for energy absorption by deformation of the waste package or drift wall and (2) the speed of impact is the largest possible speed for an earthquake of a given strength, regardless of the distance between the waste package and drift wall. In the second scenario, the clearance between the fuel assembly and the surface is small. If the clearance is small, the maximum impact speed is obtained by applying the peak ground acceleration continuously for travel across the clearance. If the clearance is small, the impact speed will be smaller than the peak ground velocity. This type of loading could occur if an intact waste package is in a collapsed drift, and the fuel assemblies strike the fuel basket.

5.2.1 Equations of Motion for a Fuel Rod

A fuel rod can be approximated as a continuous, simple beam that is supported by the spacer grids. The stiffest configuration of a beam is that with fixed ends, so that configuration absorbs the smallest amount of energy before yielding. Consider a uniform elastic beam with fixed ends under dynamic loads. Let the length of the beam be L. The supports for the beam are taken to be at $x = 0$ and $x = L$, where x is the horizontal coordinate (distance along the beam). Let the linear mass density (mass per unit length) be μ. For the end conditions considered here, the displacements and velocities of the beam are symmetric, that is, the momentum and displacement are the same at x and at $L - x$. Therefore, it is only necessary to consider half of the beam. In a continuum treatment, the Hamiltonian H_c of half the beam is

$$H_c = \int_0^{L/2} \frac{1}{2}\mu[v(\xi,\tau)]^2 d\xi + \int_0^{L/2} \frac{1}{2}k\left[\frac{\partial^2 y}{\partial \xi^2}(\xi,\tau)\right]^2 d\xi \qquad \text{(Eq. 1)}$$

Here y is the vertical coordinate (deflection of the beam), ξ is a dummy variable for integration along the horizontal coordinate, τ is time, k is a constant that describes the stiffness of the beam, and $v(\xi,\tau) = \partial y(\xi,\tau)/\partial\tau$. Note that the first term in the Hamiltonian is the kinetic energy and the second is the potential energy. In the second term, $\partial^2 y/\partial\xi^2$ is used as an approximation for the curvature of the beam. This approximation is applicable for small deflections, which are expected for fuel rods, because the rods will break before the deflections become large.

The half-beam can be approximated as a jointed chain. Let the chain consist of n links, so that each link of the chain has a length of $L/2n$ and consists of a particle of mass $m = \mu L/2n$ at the center of the link and two rigid massless beams of length $L/4n$. Between the links are linearly

elastic torsion joints. The support is at joint 0, and the middle of the span is at joint n. Joint i is at $x = iL/2n$; mass i is at $x = iL/2n + L/4n$. In this discrete approximation, the Hamiltonian H of half the beam is

$$H = \sum_{i=0}^{n-1} \frac{1}{2m} p_{i,t}^2 + \frac{1}{2} kC_{0,t}^2 \frac{L}{4n} + \sum_{i=1}^{n-1} \frac{1}{2} kC_{i,t}^2 \frac{L}{2n} + \frac{1}{2} kC_{n,t}^2 \frac{L}{4n} \qquad \text{(Eq. 2)}$$

Here the initial time is taken to be $\tau = 0$, and t is a dimensionless integer index for time so that $\tau = t\Delta\tau$, where $\Delta\tau$ is the time step. The value $p_{i,t}$ is the momentum of particle i at (dimensionless) time t, so the first term in the Hamiltonian is the kinetic energy. The potential energy requires a bit more discussion. The value of $C_{i,t}$ is the curvature of the chain at joint i and time t. Except at the ends, this curvature is taken to apply over the length of one link, that is $L/2n$, centered at the joint. To handle the ends, the curvatures at the two end joints (at $x = 0$ and $x = L/2$) are applied over a length of only $L/4n$ rather than $L/2n$.

The value of $C_{i,t}$ is determined as follows. Let $q_{i,t}$ be the vertical coordinate of mass i at time t, and let $y_{i,t}$ be the vertical coordinate of joint i at time t. For the chain approximation described above,

$$q_{i,t} = (y_{i,t} + y_{i+1,t})/2 \qquad \text{(Eq. 3)}$$

because the links are rigid. Also, to reflect the fixed ends, let the displacement at the support be zero: $y_{0,t} = 0$. By taking first differences, the slope of the beam (first derivative of the deflection) at $x = iL/2n + L/4n$ is found to be $(y_{i+1,t} - y_{i,t})(2n/L)$. By taking second differences, the curvature of the beam (second derivative of the deflection) at $x = iL/2n$ is found to be

$$C_{i,t} = (y_{i+1,t} - 2y_{i,t} + y_{i-1,t}) \frac{4n^2}{L^2} \qquad \text{(Eq. 4)}$$

Near the ends of the chain, the index for the joint may be inappropriately large ($i+1 > n$) or small ($i-1 < 0$); these cases can be handled by using symmetry: $y_{-1,t} = y_{1,t}$ and $y_{n+1,t} = y_{n-1,t}$.

From standard Hamiltonian mechanics, the equations of motion (Ref. 6) may be written as

$$\dot{q}_{i,t} = \frac{\partial H}{\partial p_{i,t}} \qquad \text{(Eq. 5)}$$

and

$$\dot{p}_{i,t} = -\frac{\partial H}{\partial q_{i,t}} \qquad \text{(Eq. 6)}$$

Here the dot indicates differentiation with respect to the actual time τ, not the dimensionless time index t. From Equations 2 and 5, it follows that

$$\dot{q}_{i,t} = p_{i,t} / m \qquad \text{(Eq. 7)}$$

The derivatives of the momenta are slightly more complex because the Hamiltonian in Equation 2 is written in terms of the curvatures $C_{j,t}$ rather than the coordinates $q_{i,t}$. If the end effects in Equation 2 are temporarily ignored, the derivatives of the momenta can be obtained by using the chain rule:

$$\dot{p}_{i,t} = -\frac{kL}{2n} \sum_{j=0}^{n} \sum_{k=0}^{n} \frac{\partial C_{j,t}}{\partial y_{k,t}} \frac{\partial y_{k,t}}{\partial q_{i,t}} C_{j,t} \qquad \text{(Eq. 8)}$$

The Jacobian matrix $\partial C_{j,t} / \partial y_{k,t}$ is obtained by differentiating Equation 4. The matrix is square, with $n+1$ rows and columns. Along the main diagonal, each element is $-8n^2/L^2$. Along the first superdiagonal and first subdiagonal, almost all the elements are $4n^2/L^2$. The only exceptions are the first element of the first superdiagonal and the last element of the first subdiagonal, which are $8n^2/L^2$ because of end effects. The remaining elements are zero.

Obtaining $\partial y_{k,t} / \partial q_{i,t}$ requires a solution to Equation 3. Using the fixed end condition $y_{0,t} = 0$, one obtains, by rearranging Equation 3,

$$y_{0,t} = 0 \qquad \text{(Eq. 9a)}$$

$$y_{1,t} = 2q_{0,t} \qquad \text{(Eq. 9b)}$$

$$\begin{aligned} y_{2,t} &= 2q_{1,t} - y_{1,t} \\ &= 2q_{1,t} - 2q_{0,t} \end{aligned} \qquad \text{(Eq. 9c)}$$

$$\begin{aligned} y_{3,t} &= 2q_{2,t} - y_{2,t} \\ &= 2q_{2,t} - 2q_{1,t} + 2q_{0,t} \end{aligned} \qquad \text{(Eq. 9d)}$$

$$\begin{aligned} y_{i+1,t} &= 2q_{i,t} - y_{i,t} \\ &= \sum_{j=0}^{i} 2q_{j,t}(-1)^{i-j} \text{ for } 0 \le i < n \end{aligned} \qquad \text{(Eq. 9e)}$$

The Jacobian matrix $\partial y_{k,t} / \partial q_{i,t}$ is obtained by differentiating Equations 9a and 9e. This matrix has $n+1$ rows and n columns. As can be seen from Equation 9a, all elements of the first row are zero. The balance of the matrix is an $n \times n$ square matrix, in which the elements are 2 along the main diagonal, –2 along the first subdiagonal, 2 along the second subdiagonal, etc. All the elements above the main diagonal are zero. It should be noted that $\partial C_{j,t} / \partial y_{k,t}$ and $\partial y_{k,t} / \partial q_{i,t}$ are both time-invariant, so they need only be evaluated once.

A combined Jacobian matrix $J_{i,j}$ can be defined such that

$$J_{i,j} = \sum_{k=0}^{n} \frac{\partial C_{i,t}}{\partial y_{k,t}} \frac{\partial y_{k,t}}{\partial q_{j,t}} \quad \text{(Eq. 10)}$$

Here the subscript t has been eliminated from $J_{i,j}$ because, as was noted previously, all the derivatives are time-independent. Note also that, since Equation 4 is linear in the vector ($y_{0,t}$, $y_{1,t}$, ..., $y_{n,t}$) and Equations 9a and 9e are linear in the vector ($q_{0,t}$, $q_{1,t}$, ..., $q_{n-1,t}$), it follows that

$$C_{i,t} = \sum_{j=0}^{n-1} J_{i,j} q_{j,t} \quad \text{(Eq. 11)}$$

The form of Equation 11 suggests defining a modified Jacobian matrix:

$$\begin{aligned} \hat{J}_{i,j} &= \frac{J_{i,j}}{\sqrt{2}} \text{ for } i = 0 \text{ and } i = n \\ &= J_{i,j} \text{ for } 0 < i < n \end{aligned} \quad \text{(Eq. 12)}$$

The Hamiltonian (Equation 2) can then be rewritten, with end effects included, as

$$H = \frac{1}{2m} \sum_{i=0}^{n-1} p_{i,t}^2 + \frac{kL}{4n} \sum_{j=0}^{n} \sum_{l=0}^{n-1} (\hat{J}_{j,l} q_{l,t})^2 \quad \text{(Eq. 13)}$$

so

$$\frac{\partial H}{\partial q_{i,t}} = \frac{kL}{2n} \sum_{j=0}^{n} \sum_{l=0}^{n-1} \hat{J}_{j,l} q_{l,t} \sum_{r=0}^{n-1} \frac{\partial}{\partial q_{i,t}} (\hat{J}_{j,r} q_{r,t}) = \frac{kL}{2n} \sum_{j=0}^{n} \sum_{l=0}^{n-1} \hat{J}_{j,l} q_{l,t} \sum_{r=0}^{n-1} \hat{J}_{j,r} \frac{\partial q_{r,t}}{\partial q_{i,t}} \quad \text{(Eq. 14)}$$

But $\partial q_{r,t} / \partial q_{i,t} = \delta_{ri}$, where δ_{ri} is the Kronecker delta ($\delta_{ri} = 1$ for $r = i$; $\delta_{ri} = 0$ for $r \neq i$), and

$$\sum_{r=0}^{n-1} \hat{J}_{j,r} \delta_{ri} = \hat{J}_{j,i} \quad \text{(Eq. 15)}$$

so, from Equations 6, 14, and 15, it follows that

$$\dot{p}_{i,t} = -\frac{kL}{2n} \sum_{j=0}^{n} \sum_{l=0}^{n-1} \hat{J}_{j,l} q_{l,t} \hat{J}_{j,i} = -\frac{kL}{2n} \sum_{l=0}^{n-1} \sum_{j=0}^{n} \hat{J}_{i,j}^{T} \hat{J}_{j,l} q_{l,t} \quad \text{(Eq. 16)}$$

Note that the sum over j is invariant and need only be evaluated once. Equations 7 and 16 constitute a complete set of equations of motion.

5.2.2 Stiffness of a Fuel Rod

To determine the flexural stiffness constant k, it is necessary to describe how the fuel rods absorb energy as they bend. Let dU be the potential energy of an element of length dL of an elastically bent fuel rod. If the slope of the fuel rod is small, the curvature of the fuel rod may be approximated by the second derivative of the transverse displacement with respect to distance along the fuel rod, so

$$dU = \frac{1}{2}k\left(\frac{\partial^2 y}{\partial x^2}\right)^2 dL \qquad \text{(Eq. 17)}$$

where k is a constant, x is the distance along the fuel rod, and y is the transverse displacement of a point on the rod. Note that k is for bending of a fuel rod; it is not the "spring constant" that is commonly used for uniaxial strain.

The potential energy of a uniaxially loaded elastic element of volume dV is $\sigma\varepsilon dV/2$, where σ is the stress and ε is the strain. But $\sigma = E\varepsilon$, where E is the elastic modulus, so the potential energy is $E\varepsilon^2 dV/2$.

The relationship between the curvature and the strain for a given fiber is obtained as follows. Suppose that a length of rod is bent with a radius of curvature ρ to form an arc of angle ϕ. The length of the neutral axis remains invariant at $\rho\phi$. For thin-walled cladding, the tensile side has a larger radius of curvature, $\rho + R_m$, where R_m is the midwall radius of the cladding. Therefore, the tensile side is extended to a length $(\rho + R_m)\phi$. The resulting strain is R_m/ρ. Let θ be an angular parameter for a location around the circumference of the fuel rod so that the tensile side of the cladding corresponds to $\theta = \pi/2$. From the geometric argument above, it is clear that the strain at angle θ is

$$\varepsilon(\theta) = \frac{R_m}{\rho}\sin\theta \qquad \text{(Eq. 18)}$$

The total potential energy dU of an element of cladding of length dL is then

$$\begin{aligned} dU &= 2\int_{\theta=-\pi/2}^{\pi/2} \frac{E\varepsilon^2(\theta)}{2} wR_m d\theta dL = EwR_m \int_{\theta=-\pi/2}^{\pi/2} \frac{R_m^2}{\rho^2}\sin^2\theta\, d\theta dL \\ &= \frac{EwR_m^3}{\rho^2}\int_{\theta=-\pi/2}^{\pi/2}\sin^2\theta d\theta dL = \frac{EwR_m^3\pi}{2\rho^2}dL \end{aligned} \qquad \text{(Eq. 19)}$$

where w is the thickness of the cladding. In evaluating the integral in Equation 19, it was noted that $\sin^2\theta = (1-\cos 2\theta)/2$. Since the interval of integration covers exactly one wavelength of the cosine, the positive and negative contributions of the cosine cancel each other. By noting that $1/\rho = (\partial^2 y/\partial x^2)$, and combining Equations 17 and 19, it follows that

$$k = \pi E w R_m^3 \qquad \text{(Eq. 20)}$$

5.2.3 Solution to Equations of Motion and Resulting Strains

Attachment I shows a method for solving the equations of motion for a span of a fuel rod with fixed ends. The geometry of a W1717WL fuel assembly is used. Two of the inputs to the Mathcad workbook in Attachment I are specified by the user: the number of links in half the chain n and the time step $\Delta\tau$ that is used for solving the differential equations. The following strategy is used in choosing n and $\Delta\tau$. In general, larger values of n are expected to provide a better description of an elastic beam because a chain with many elastic joints is a better approximation of a continuum than is a chain with only a few joints. However, it is common in solving partial differential equations that a system with fine spatial divisions requires small time steps; large time steps lead to instability. If Equations 7 and 16 are solved exactly, the Hamiltonian will be time-independent. For the calculations reported here, the time step was considered to be small enough, and the solution precise enough, if the Hamiltonian at the end of the time period of interest (H_f) differed by less than 1% from the original value (H_0). This criterion was met for each of the calculations reported here. Values of n, $\Delta\tau$, and H_f / H_0 are given in Table 1.

The time period of interest reflects the type of contact that would exist between the fuel assembly and the unyielding surface. If the spacer grids were stuck to the unyielding surface, the fuel rods would oscillate, and the spacer grids would alternately push and pull on the surface. For impact, however, the spacer grids are only in contact with the unyielding surface, not fastened to it. Rather than pulling on the surface, the spacer grids would simply lift off. Therefore, the period of interest is only that period when the fuel rods are deflected toward the surface. For the calculations reported here, the fuel rod was taken to start in a stress-free state. Upon impact, the rod begins to deflect. The average deflection over the span starts at zero, decreases (becomes negative), reaches a minimum, and then increases. The period of interest was taken to end when the average deflection returns to zero.

The solution to the equations of motion allows us to calculate the bending stress. For a given time t and distance x from the end of the fuel rod, the bending stress in the cladding is

$$\sigma(x,\phi,\tau) = -EC(x,\tau)vR\sin\phi \qquad \text{(Eq. 21)}$$

where R is the cladding radius, C is the instantaneous curvature of the fuel rod for impact at unit speed, x is the distance from the support, τ is time, v is the impact speed, and E is the elastic modulus. Here ϕ is the angular position around the cladding, defined so that $\phi = 0$ and $\phi = \pi$ correspond to the neutral axis, $\phi = \pi/2$ corresponds to the part of the fuel rod farthest from the unyielding surface, and $\phi = 3\pi/2$ corresponds to the part of the fuel rod closest to the surface. Note that the curvature and stress are linear in the impact speed; this follows because the cladding is treated as being linearly elastic. The time dependence of $\sigma(x, \phi, \tau)$ is not of particular interest; to determine whether the cladding will fail, it is sufficient to examine only the minimum and maximum stresses.

Table 1. Values of n, $\Delta\tau$, and H_f / H_0 for Calculations of Fuel Rod Impact

n	$\Delta\tau$ (μs)	H_f / H_0
3	40	0.99974
4	20	0.99919
5	10	0.99909
6	4	0.99982
7	4	0.99812
8	4	0.99291
9	2	0.99725
10	2	0.99501
11	2	0.99569
12	2	0.99602
13	2	0.99561
14	2	0.99478
15	2	0.99464
16	2	0.99431
17	1	0.99645
18	1	0.99638
19	1	0.99624
20	1	0.99595
21	0.8	0.99649
22	0.8	0.99630
23	0.6	0.99697
24	0.6	0.99683
25	0.5	0.99716
26	0.5	0.99707
27	0.4	0.99747
28	0.4	0.99738
29	0.3	0.99786
30	0.3	0.99780
31	0.25	0.99804
32	0.25	0.99798

Since the minimum and maximum stresses are of such importance, it is important that the minimum and maximum curvatures be calculated as accurately as possible. Two approaches to this are illustrated in Figures 1 and 2. Figure 1 shows the maximum and minimum curvature, for impact at −1 m/s, as a function of position, for various values of n. The horizontal axis of Figure 1 matches the horizontal coordinate in the calculation. The left end of the axis is at the support; the right end is at midspan.

The first approach to accurate calculation of curvatures is to use the results for the largest value of n because larger values of n would be expected to provide the most accurate results. With this approach, the curve for $n = 32$ in Figure 1 should be used because this is the largest value of n that was considered. (Significantly larger values of n would have exceeded the memory-handling limits of Mathcad.) The smoothness of the plot on page I-5 indicates that the shape of the deformed beam is well represented even at $n = 16$; therefore, there is little motivation to extend the calculation to values of n beyond those considered here.

The second approach is to extrapolate from the available results to infinite n. In Figure 1, it is apparent that the disparity between the results for $n = 4$ and $n = 32$ is greatest for the minimum curvature at the support. The disparity may also be large for the maximum curvature at the support and for the minimum and maximum curvatures at midspan. Figure 2 illustrates an approach to extrapolation. In this figure, the minimum and maximum curvatures at the support and at midspan are plotted as a function of $1/n$. The data points correspond to the endpoints of the curves in Figure 1, but in Figure 2, results are given for more values of n. For $n = 4$ through $n = 20$, there appears to be a trend in which the curvature varies linearly with $1/n$. However, for larger values of n, the trend for the curvatures at the support seems to be different.

It should be noted that, except at the endpoints, extrapolation is usually impractical because calculations for different values of n consider different positions along the fuel rod. The support and midspan are unusual in that these locations are considered for all values of n.

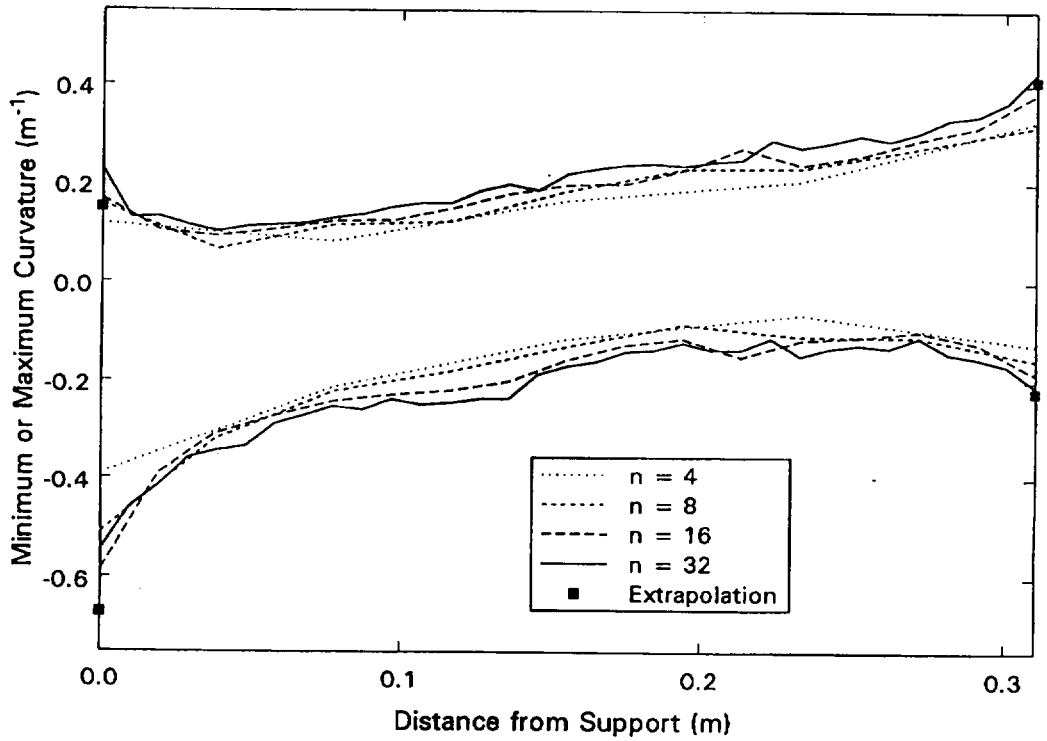

Figure 1. Minimum and Maximum Fuel Rod Curvatures as a Function of Position

The approach used here is a combination of the two approaches described above. Since extrapolation is impractical, the general approach is to use the curvature profile as calculated for $n = 32$. However, when the extrapolations in Figure 2 predict a larger magnitude for the curvature, the extrapolated value is used instead. From the extrapolations in Figure 2, it is estimated that the minimum curvatures at the support and midspan are -0.67 m^{-1} and -0.22 m^{-1}, respectively. These have greater magnitude than the curvatures calculated with Attachment I, so

they are used rather than the calculated values. The overall results are tabulated in Attachment II. Each line of Attachment II describes the results for one of the point masses in the chain. Each line contains six values. They are, respectively, the total number of links in the chain n, the time step $\Delta\tau$, the ratio of Hamiltonians H_f / H_0, the distance of the mass from the support (in meters), and the minimum and maximum curvatures (in reciprocal meters) at that position for impact at −1 m/s. The minimum curvatures at the support and at midspan, as listed in Attachment II, have been modified to the extrapolated values. Relevant output from the Mathcad workbook is documented in Figures 1 and 2 and in Attachment II. Other output values were not used and are not documented.

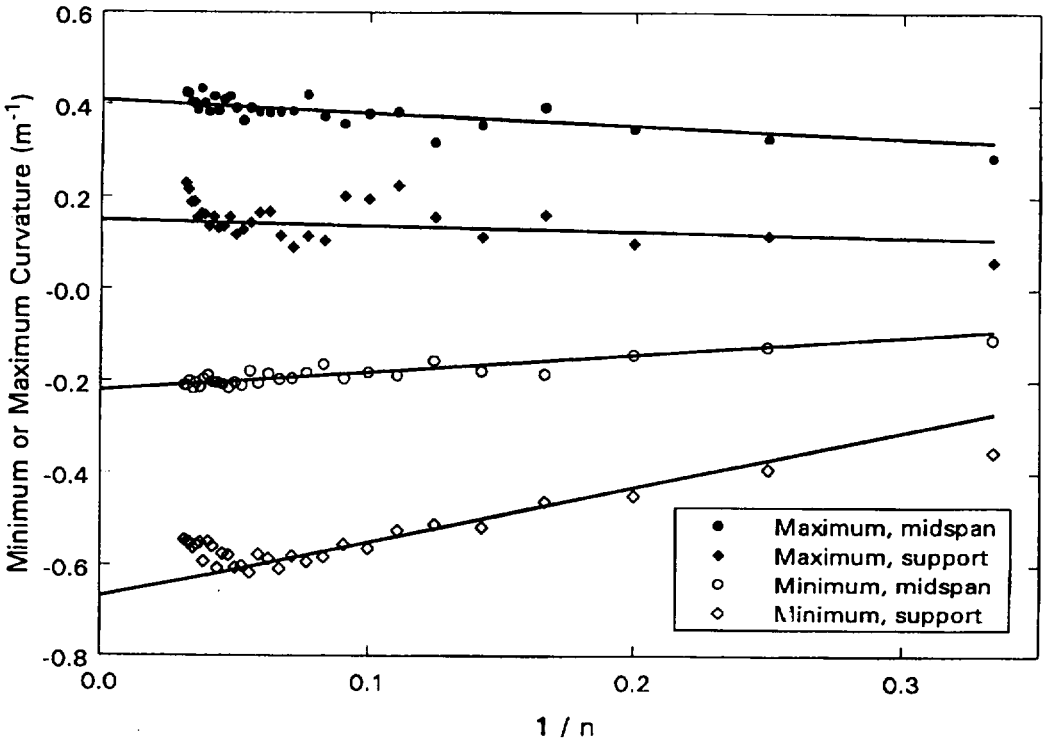

Figure 2. Minimum and Maximum Curvatures at Support and Midspan for Various Values of n

5.2.4 Loading Scenarios

As was mentioned in Section 5.2, two loading scenarios are considered here. In both scenarios, a fuel assembly is taken to impact on a flat, unyielding surface. The fuel assembly is taken to remain in one place because of inertia, while the surface strikes the assembly because of ground motion. The two differ in the way that the velocity of impact is determined. In Scenario 1, the impact occurs at the peak ground velocity. In Scenario 2, the impact occurs at a velocity of

$$v = \sqrt{2Ax} \qquad \text{(Eq. 22)}$$

where A is the peak ground acceleration and x is the displacement that is possible before impact. The velocity of impact for Scenario 2 is what would be obtained if the peak ground acceleration were applied throughout the displacement. Note that there are two *independent* upper limits on the impact velocity: the peak ground velocity (Scenario 1) and $(2Ax)^{1/2}$ (Scenario 2). In any seismic event, neither of these limits can be exceeded. Therefore, the correct scenario is the one that provides the *smaller* impact velocity. If the available displacement is large, there is plenty of room for acceleration of the surface, but the velocity of the surface can nevertheless not exceed the peak ground velocity. On the other hand, if the displacement available between the fuel assembly and the surface is small, the impact velocity is also necessarily small because there is little room for the surface to accelerate before striking the assembly. The velocity of impact is therefore limited by the peak ground acceleration and displacement rather than the peak ground velocity.

Scenario 1 is appropriate when large displacements are possible. It would apply to an intact waste package in an open drift. In this case, horizontal ground motion could cause a drift wall to strike a waste package at the peak ground velocity. The containment barriers and basket would accelerate very quickly to the peak ground velocity and could strike the assemblies, which would still be at rest.

Scenario 1 would also apply, regardless of whether the drift is open, to a waste package with a degraded basket but containment barriers that generally retain their original geometry. If the basket is degraded, the fuel assemblies can move long distances within the waste package before striking the inner surface of the containment barriers.

Scenario 2 would apply to an intact waste package in a rubble-filled drift. In this case, the containment barriers and basket would accelerate along with the ground. Since there is only a small clearance between the fuel assembly and basket, the basket would not be able to accelerate much before striking the assembly.

For simplicity, horizontal and vertical ground motions are taken as independent hazards. Both are treated by applying the peak ground motion to a fuel assembly that is at rest. Only ground motion perpendicular to the drift is considered; motion parallel to the drift will not cause the waste packages to strike anything.

5.2.5 Failure Mechanisms

When the fuel assembly strikes a surface, either of two failure mechanisms may apply: rupture and fracture. The simpler of these is rupture. In general, a ductile fuel rod would bend elastically, then plastically, until the failure strain is reached. At this point, the rod would fail. Since a dynamic treatment of plasticity requires substantial computation, this calculation considers only elastic deformation, that is, a fuel rod is taken to fail when the yield strength in bending is exceeded. Rupture is a particularly simple failure mechanism because exceeding the bending strength at any point is always treated as causing failure. From Equation 21, it follows that the largest stresses occur where the magnitude (absolute value) of the curvature reaches its largest value. The minimum and maximum curvatures have been tabulated as functions of distance from

the support. The fifth and sixth columns of Attachment II give these curvatures for an impact at −1 m/s. The curvature with the largest magnitude is $-0.67\ m^{-1}$. Therefore, Equation 21 can be rearranged to give the following criterion for failure by rupture: $0.67\ s \cdot m^{-2} \cdot ERv > \sigma_y$. Here σ_y is the yield strength in bending, the other variables are as defined in Section 5.2.3, and the coefficient $0.67\ s \cdot m^{-2}$ is the ratio of the curvature to the impact speed. Alternatively, the probability of failure by rupture for a fuel rod (or fragility) is

$$P_{frr} = \Phi\left(\frac{0.67\,s \cdot m^{-2} ERv}{\sigma_y} - 1\right) \qquad \text{(Eq. 23)}$$

where Φ is the Heaviside step function ($\Phi(x) = 1$ for $x \geq 0$; $\Phi(x) = 0$ for $x < 0$).

Failure by fracture is more complicated because stress and the existence of a preexisting flaw must both be considered. For side loading of a fuel assembly, bending of the fuel rods produces tensile stresses that can cause mode I (crack opening) fracture.

Consider the following distribution of flaw sizes:

$$P(s) = \int_s^{\infty} Be^{-Bx} dx = e^{-Bs} \qquad \text{(Eq. 24)}$$

where $P(s)$ is the probability that a given flaw will have a depth greater than or equal to s and B is a parameter that describes the depth of a typical flaw. This distribution is well suited for cladding flaws since it uses only one parameter (B) and cladding flaws are generally not well characterized. It is noted that $P(0) = 1$, that is, any flaw is assured of having a depth of at least zero. The use of ∞ as an upper limit of integration is an approximation. Flaw sizes cannot be larger than the cladding thickness, but the portion of the distribution with larger flaw sizes is so small that it has a negligible effect.

The parameter B has been estimated as follows. For a randomly chosen flaw, the probability that it has a size less than s is $1 - P(s)$. For a whole rod with N flaws, the probability that all the flaws are smaller than size s is $[1 - P(s)]^N$. Therefore, the probability that at least one flaw has a size greater than or equal to s is $1 - [1 - P(s)]^N$. Let $P_{fail}(s)$ be the probability that a fuel rod with a flaw of size s will fail in reactor from pellet-clad interaction. The critical flaw size A_{crit} (the size for which $P_{fail}(A_{crit}) = ½$) has been determined to be $A_{crit} = 0.28b$, where b is the cladding thickness (Section 5.1). For W1717WL cladding, $b = 0.5715$ mm (Section 5.1). Finally, the frequency of rod failure due to pellet-clad interaction has been estimated as $A_{freq} = 10^{-4}$ (Section 5.1), and the number of pellet-clad interaction flaws per fuel rod has been estimated as $N = 60$ (Section 5.1). These results are combined as follows:

$$P_{fail}(A_{crit})[1 - [1 - P(A_{crit})]^N] = A_{freq} \qquad \text{(Eq. 25)}$$

This can be rearranged and then combined with Equation 24 to yield

$$P(A_{crit}) = 1 - \left(1 - \frac{A_{freq}}{P_{fail}(A_{crit})}\right)^{1/N} = e^{-BA_{crit}} \qquad \text{(Eq. 26)}$$

Finally, by solving for B and using $P_{fail}(A_{crit}) = \frac{1}{2}$, it follows that

$$B = -\ln[1 - (1 - 2A_{freq})^{1/N}] / A_{crit} \qquad \text{(Eq. 27)}$$

For the values of N, A_{crit}, and A_{freq} given above, $B = 7.9 \times 10^4\ \text{m}^{-1} = 0.079\ \mu\text{m}^{-1}$.

The mode I (crack opening) stress intensity factor K_I for a semi-elliptical crack will depend on the remote bending stress in the outer fiber σ, the crack depth a, the cladding thickness b, the crack width c, and the outer radius of the cladding R. Ref. 18 gives the following equation for K_I:

$$K_I = \sigma \sqrt{\frac{\pi a}{Q}} F \qquad \text{(Eq. 28)}$$

where $Q = 1 + 1.464(a/c)^{1.65}$ and F is a function of a/c, a/b, R/b, and location along the front of the crack. The function F is tabulated in the lower part of Ref. 19. The values of a/c and a/b are not known and will vary from crack to crack, but for all tabulated values, $F/Q^{1/2} < 1$. Therefore it is conservative to simplify Equation 28 to

$$K_I = \sigma \sqrt{\pi a} \qquad \text{(Eq. 29)}$$

A crack will propagate if $K_I > K_{Ic}$, where K_{Ic}, is the critical mode I stress intensity (fracture toughness) of the material.

During the impact, the fuel rods will start straight, deform as the spacer grids strike the surface and the rods decelerate, and then spring back. As the rods rebound, the assembly will be lifted off the surface. To describe the limited time for interaction of the assembly with the unyielding surface, the current calculation considers motion of the rods only until the average deflection of the rods returns to zero. During this period, the curvature of the fuel rod depends in a complicated way on time and distance from the spacer grids.

For specificity, consider a fuel rod that is moving downward with a velocity of 1 m/s when the spacer grids strike the surface. As each rod decelerates, it will be deflected downward, and it will generally have negative curvature (concave downward) near the grids and positive curvature (concave upward) near midspan. At any particular position along the rod, however, high-frequency oscillations could cause the curvature to be positive at some times and negative at others. Positive curvatures will impose tensile stresses on the lower half of the cladding and compressive stresses on the upper half. Negative curvatures produce the opposite pattern. However, only tensile stresses cause crack propagation; compressive stresses are benign as regards fracture.

The stress as a function of time and position is given in Equation 21. Since it is the largest tensile (most positive) stress that determines the smallest flaw that will grow, one can define two functions $C_{max}(x)$ and $C_{min}(x)$, which are the maximum and minimum values of $C(x,\tau)$ over the period of impact for point x. The stress that is of interest in predicting whether a crack will grow is then $\sigma_{mod}(x, \phi)$, where

$$\begin{aligned} \sigma_{mod}(x,\phi) &= -EC_{min}(x)vR\sin\phi \quad \text{for} \quad 0 \le \phi < \pi \\ &= -EC_{max}(x)vR\sin\phi \quad \text{for} \quad \pi \le \phi < 2\pi \end{aligned} \qquad \text{(Eq. 30)}$$

Note that $\sigma_{mod}(x,\phi) \ge 0$ for all x and ϕ. This can be proved as follows. First, note that $C(x,0) = 0$ for all x. Therefore, for all x, $C_{max}(x) \ge 0$ and $C_{min}(x) \le 0$. But $\sin\phi$ is negative when it is multiplied by $C_{max}(x)$ and positive when it is multiplied by $C_{min}(x)$. Therefore, $\sigma_{mod}(x,\phi) \ge 0$ for all x and ϕ.

Having defined $\sigma_{mod}(x,\phi)$, it follows from Equation 29 that

$$a_{cr}(x,\phi) = \frac{K_{Ic}^2}{\pi\sigma_{mod}{}^2(x,\phi)} \qquad \text{(Eq. 31)}$$

where a_{cr} is the size of the critical flaw.

Given that there are N flaws over the active length λ of the rod, the probability of having a flaw in an element of surface area with length dx and angular extent $d\phi$ is $N\,dx\,d\phi/2\pi\lambda$. Since the element is of infinitesimal area, the probability of having more than one flaw may be neglected. The probability of failure of this element of area is then the product of the probability of having a flaw and the probability that a given flaw is larger than a_{cr}. For a given loading, the probability P_{fef} of failure of an element of area by fracture is

$$P_{fef} = \frac{N\,dx\,d\phi}{2\pi\lambda}\exp\frac{-BK_{Ic}^2}{\pi\sigma_{mod}{}^2(x,\phi)} \qquad \text{(Eq. 32)}$$

The probability of survival is one minus the probability of failure. To obtain the probability that an entire rod will survive without fracture, it is necessary to multiply the probabilities of survival for all the elements of area. This can be done as follows. By making a Taylor series expansion of the natural logarithm about 1 and keeping only the linear term ($\ln(1+\delta) \approx \delta$), it is found that the logarithm of the probability of survival against fracture P_{sef} of an element of area as $\ln(P_{sef}) = -P_{fef}$. For a whole rod, the logarithm of the probability of survival P_{srf} is the integral over the rod of the probability of survival of the elements:

$$\ln(P_{srf}) = \int_{x=0}^{\lambda}\int_{\phi=0}^{2\pi}\frac{-N}{2\pi\lambda}\exp\left(\frac{-BK_{Ic}^2}{\pi\sigma_{mod}{}^2(x,\phi)}\right)d\phi\,dx \qquad \text{(Eq. 33)}$$

By applying the definition of σ_{mod} (Equation 30) and taking exponentials on both sides, Equation 33 becomes

$$P_{srf} = \exp\left[\frac{-N}{2\pi\lambda}\int_{x=0}^{\lambda}\int_{\phi=0}^{\pi}\left[\exp\left(\frac{-cf}{(C_{min}(x)\sin\phi)^2}\right)+\exp\left(\frac{-cf}{(C_{max}(x)\sin\phi)^2}\right)\right]d\phi\,dx\right] \quad \text{(Eq. 34)}$$

where

$$c = \frac{B}{\pi E^2 R^2} \quad \text{(Eq. 35)}$$

and

$$f = \frac{K_{Ic}^2}{v^2} \quad \text{(Eq. 36)}$$

The single parameter f includes the effects of both the fracture toughness of the cladding and the speed of impact. In writing Equation 34, the interval of integration from $\phi = 0$ to $\phi = \pi$ was combined with the interval from $\phi = \pi$ to $\phi = 2\pi$ by noting that $\sin^2(\phi+\pi) = \sin^2\phi$.

Note that the outer integral in Equation 34 covers the entire active length of the rod. In contrast, the dynamic beam calculations cover only half of the span from one spacer grid to the next. Since each half span should be similar, the limits of integration for x can be changed to 0 and $L/2$, where L is the maximum distance between spacer grids, and the reduction of the interval of integration can be offset by multiplying the integral by the number of half spans, which is $2\lambda/L$. Therefore

$$P_{srf} = \exp\left[\frac{-N}{\pi L}\int_{x=0}^{L/2}\int_{\phi=0}^{\pi}\left[\exp\left(\frac{-cf}{(C_{min}(x)\sin\phi)^2}\right)+\exp\left(\frac{-cf}{(C_{max}(x)\sin\phi)^2}\right)\right]d\phi\,dx\right] \quad \text{(Eq. 37)}$$

The probability of failure of a rod P_{frf} is just the complement of this:

$$P_{frf} = 1 - P_{srf} \quad \text{(Eq. 38)}$$

In Attachment III, P_{frf} is calculated as a function of f. The results are saved in a file for later use; the file is tabulated in Attachment IV. Each line of Attachment IV contains two values: a value of the parameter f and the corresponding probability of failure of a fuel rod, respectively.

5.2.6 Seismic Risk

This section discusses the seismic hazard, then shows how this quantity is combined with the fragility to yield the seismic risk. The seismic hazard has been given as $H(s)$ where s is a measure of the strength of ground motion (such as peak ground velocity or peak ground acceleration) and H is the annual probability of exceedance for that strength. That is, $H(s)$ is the probability that an earthquake of strength s or larger will occur during a given year. $H(s)$ is similar to a cumulative distribution function, though cumulative distribution functions normally give the probability that a given quantity will be less than or equal to a given value. From $H(s)$, the probability of an earthquake of a given strength can be calculated. For an infinitesimal interval of strengths from s to $s+ds$, the probability of an earthquake with a strength that falls in this interval is $-(dH(s)/ds)\,ds$.

The seismic hazard works with the fragility, which was determined in Section 5.2.5. Let $P_{fr}(s)$ be the probability of failure for a fuel rod that is exposed to an earthquake of strength s. The rate of failure of fuel rods is obtained by calculating the probability of an earthquake of strength s, multiplying that by the probability of failure given that an earthquake of strength s has occurred, and adding the contributions for all strengths. That is,

$$R = -\int_0^{s_{max}} \frac{dH(s)}{ds} P_{fr}(s)\,ds \qquad \text{(Eq. 39)}$$

where s_{max} is an upper cutoff point for the integral and R is the seismic risk. R gives the expected fraction of fuel rods broken per year. Equation 39 is a convolution of the seismic hazard with the fragility. The ground motion strength s_{max} has an annual probability of exceedance of 10^{-8} yr^{-1}; less frequent earthquakes are neglected.

The integral in Equation 39 requires consideration of stronger ground motions than those documented in Ref. 12, so the seismic hazard curves were extrapolated linearly on semi-log axes (logarithm of annual probability of exceedance vs. ground motion strength). This treatment is expected to be conservative because the results in Ref. 12 are based on an analysis in which it is assumed that rock behavior is linear. In fact, nonlinear behavior of the rock, such as crushing and fracturing, will absorb energy in very strong earthquakes and will weaken the ground motion.

It should be noted that, in the treatment above, the fragility does not change with time. In fact, one would expect that the most fragile rods would break early, in earthquakes of modest strength, and the population of rods that remain intact would become less fragile with time. This "survival of the fittest" effect has been neglected. This is a conservative simplification.

The application of Equation 39 depends on the particular hazard and loading scenario being considered. For Scenario 1 (as defined in Section 5.2.4), the appropriate measure of strength is the peak ground velocity (horizontal or vertical), and the appropriate fragilities are P_{frr} and P_{frf} as defined in Equations 23 and 38, respectively. For Scenario 2, the fragilities are unchanged, but

the appropriate measure of strength is the peak ground acceleration (horizontal or vertical), and the impact velocity is calculated by applying Equation 22.

Seismic risks are evaluated in Attachment V. The total risk for all combinations of scenario, failure mechanism, and direction of ground motion is 1.1×10^{-6} yr^{-1}.

5.3 STATIC LOADING

At very long times, the emplacement drifts may collapse and the metallic engineered barriers may degrade to the point that spent nuclear fuel assemblies are directly exposed to the static loads from rubble in the drifts. In this section, the resistance of fuel cladding to such loads is calculated and compared to rubble loads.

5.3.1 Strength of Fuel Cladding

For elastic loading, simple beam theory can be used to determine the strength of a fuel rod. The moment of inertia I is (Ref. 20)

$$I = \frac{\pi}{4}(R^4 - R_i^4) \qquad \text{(Eq. 40)}$$

where R is the outside radius of the cladding and R_i is the inside radius. The fuel rod will yield (Ref. 21) when

$$\sigma_y = \frac{MR}{I} \qquad \text{(Eq. 41)}$$

where σ_y is the yield strength in bending and M is the bending moment. For a tubular beam, R is the distance from the neutral axis to the outer fiber.

Since the rubble in a drift may be in large pieces, it is reasonable to approximate the rubble loading by a point load. For conservatism, the load is taken to be at a distance of $L/3$ from the support. Such a loading provides a maximum bending moment (Ref. 22) of

$$M = 0.1481 mgL \qquad \text{(Eq. 42)}$$

where m is the mass resting on the fuel rod, g is the acceleration due to gravity, and L is the length of the span. Since only the magnitude of the bending moment is of interest here, the negative sign in Ref. 22 has been deleted.

For a fuel assembly overlain by rubble, the mass that would be expected to rest on one span of one rod is

$$m = sHL\rho\psi \qquad \text{(Eq. 43)}$$

where m is the mass, s is the rod spacing, H is the height of the rubble pack, ρ is the density of solid rock, and ψ is the fractional density of the rubble. Equation 43 is based on a hydrostatic approximation; the mass assigned to one fuel rod is the mass of a rectangular prism of rubble with dimensions $s \times H \times L$ and a mean density of $\rho\psi$.

Equation 43 can be solved for H and combined with Equations 40 through 42. The result is

$$H = \frac{\pi \sigma_y}{4 \cdot 0.1481 R g L^2 s \rho \psi} (R^4 - R_i^4) \qquad \text{(Eq. 44)}$$

The following values are given in Section 5.1: $\sigma_y = 1.55$ GPa, $R = (9.4996 \text{ mm})/2$, $R_i = (9.4996 \text{ mm})/2 - 0.5715$ mm, $g = 9.80665$ m/s^2, $L = 620.52$ mm, $s = 12.5984$ mm, $\rho = 2270$ kg/m^3, and $\psi = 0.60$. By using these values in Equation 44, it is found that $H = 5.45$ m. Thus, if $H \geq 5.45$ m, the fuel rods will fail in bending if σ_y is taken to be the failure stress.

5.3.2 Height of Rubble Pack

As the ground support degrades, and the emplacement drifts are shaken by earthquakes, it is reasonable to expect that the drifts will collapse and fill with rubble. This process can continue until the drift and the overlying rock volume from which the rubble falls are both filled with rubble. For the purposes of this calculation, the rubble can be approximated by a continuum with density $\rho\psi$, where ρ is the density of the rock mass and ψ is the fractional density of the rubble pack.

The height of the rubble pack will depend on the shape of the collapsed region. In Attachment VI, sketches are provided of three possible configurations: rectangular, elliptical, and triangular. As is discussed in the attachment, the height of collapse is characterized by a dimensionless quantity h, which is the height of the collapsed region above the original crown for a drift of unit radius. (Alternatively, h is the height of the collapsed region divided by the drift radius.) All three configurations are considered here.

The height of collapse is determined by applying the principle of conservation of matter. Let A_o be the original cross-sectional area of the completely empty drift. Since the drift is circular with unit radius, $A_o = \pi$. Even before collapse, some fraction f of the cross-sectional area of the drift will be filled with emplaced material. Possible types of material include fuel assemblies, backfill, and corrosion products from engineered barriers. Let $A_c(h)$ be the cross-sectional area of the region above the drift that collapses and provides material for the rubble. Then, by conservation of matter,

$$\psi [A_c(h) + A_o - A_o f] = A_c(h) \qquad \text{(Eq. 45)}$$

Both sides of Equation 45 represent the amount of rubble. On the right side, $A_c(h)$ is the cross-sectional area of the rock that is turned to rubble. The original rock has a fractional density of one. On the left side, $A_c(h) + A_o - A_o f$ is the cross-sectional area of the resulting rubble; it is the area from which the rock was taken ($A_c(h)$) plus the empty cross-sectional area of the original

drift ($A_o - A_a f$); all of this area is filled with rubble with a fractional density of ψ. Equation 45 has been solved to determine the value of h; the solutions are shown in Attachment VI.

The results in Attachment VI show that the triangular configuration gives the largest value of h, the rectangular configuration gives the smallest value, and the elliptical configuration gives an intermediate value. It could be argued that the triangular configuration is the most realistic of the three because the angle of overhang is constant on the upper surface of the collapsed region. A constant angle of overhang might be expected because a more severely overhanging wall would be expected to be more unstable, and therefore collapse more rapidly, than a less severely overhanging wall. The rectangular configuration is clearly unrealistic because a drift with a flat crown would be even less stable than a circular drift.

For the three configurations, the height of the rubble as measured from the invert of the drift varies from 8.1 m to 13.2 m (Attachment VI). If the density of the rubble from the emplaced material is similar to the density of the rubble from drift collapse, these depths can be compared with the depth provided in Section 5.3.1. It should be noted that the treatment here uses the approximation of uniform loading by the rubble. If the rubble includes large chunks, the loads may be substantially larger in some locations. However, the heights of the rubble bed calculated in this section (8.1 m to 13.2 m) are much larger than the height that an assembly can support (5.45 m, Section 5.3.1). As a result, reasonable uncertainties in the density of solid rock, fractional density of rubble, and drift diameter would not affect the results.

6. RESULTS

The results presented in this calculation are subject to TBV-3480 and TBV-3481.

This section collects results that appear in the text and attachments and discusses how uncertainty in the data affects or does not affect the results. All of the results in the following subsections are for a W1717WL fuel assembly.

6.1 SEISMIC LOADING

Seismic risks were calculated for two loading scenarios. In Scenario 1, the fuel assembly strikes an unyielding surface at the peak ground velocity. In Scenario 2, the fuel assembly strikes an unyielding surface at a velocity that is determined by peak ground acceleration and the clearance between the fuel assembly and the basket. For each scenario, fragilities were determined for both rupture and fracture, and seismic risks for both horizontal and vertical ground motions were calculated.

The results, as calculated in Attachment V but rounded to one decimal place, are summarized in Table 2. The total seismic risk for fuel rod breakage is 1.1×10^{-6} yr^{-1}. (This value reflects rounding of the terms that were added.) The largest contribution to the total risk, 9.5×10^{-7} yr^{-1}, was for Scenario 1 with horizontal ground motion and failure by fuel rod rupture. This is more than an order of magnitude larger than the second largest risk, 1.3×10^{-7} yr^{-1}, which was for Scenario 1 with vertical ground motion and failure by fuel rod rupture. Of the remaining risks, the largest is more than three orders of magnitude smaller than the total risk.

Table 2. Seismic Risks for Fuel Rod Failure

Loading Scenario	Failure Mechanism	Direction of Ground Motion	Seismic Risk (yr^{-1})
1	Rupture	Horizontal	9.5×10^{-7}
1	Rupture	Vertical	1.3×10^{-7}
1	Fracture	Horizontal	7.7×10^{-10}
1	Fracture	Vertical	1.6×10^{-10}
2	Rupture	Horizontal	0
2	Rupture	Vertical	0
2	Fracture	Horizontal	1.5×10^{-20}
2	Fracture	Vertical	1.7×10^{-21}
Total			1.1×10^{-6}

The seismic risk due to fracture is a very small part of the total risk, which is about one part in 1000. The fracture contribution is small even though a very conservative (fifth percentile) value was chosen for the fracture toughness. Since the fracture toughness was chosen conservatively and fracture makes a very small contribution to risk, it is argued that the various fracture properties (fracture toughness, number of pellet-clad interaction flaws per pressurized water reactor fuel rod, frequency of rod failure by pellet-clad interaction, and size of critical flaw as a fraction of cladding thickness) do not affect the results.

The argument above is appropriate because the fragility for failure by fracture is a continuous function. In contrast, the fragility for rupture is a Heaviside step function, so it is important to determine whether a change in the data could move the step and thus cause a different result. The risks for Scenario 2 and failure by rupture were zero for both horizontal and vertical ground motion. This result reflects the truncation of the calculation at very strong ground motions, as shown in Equation 39. Even if ground motion that is so strong that the annual probability of exceedance is 10^{-8} yr^{-1}, the relative velocity of the fuel assembly and the basket is insufficient to cause any fuel rods to rupture. From Attachment V, it can be seen that the gap between the fuel assembly and the fuel basket tube is 12.4 mm, and, for the maximum acceleration, *ahmax*, the impact speed is 1.266 m/s. In contrast, the speed necessary to rupture a rod, *vrup*, is 3.347 m/s. Since the impact speed varies with the square root of the gap, the gap necessary for impact at a speed of 3.347 m/s is 12.4 mm $\times$ $[(3.347 \text{ m/s})/(1.266 \text{ m/s})]^2 = 87$ mm. This large a gap is not credible because it would result in an unrealistic increase in waste package diameter. Therefore, the inside width of a pressurized water reactor fuel basket tube does not affect the results.

6.2 STATIC LOADING

It was calculated that an exposed fuel rod could sustain a rubble load with a depth of 5.45 m (Section 5.3.1) if the yield stress is also taken to be the failure stress. However, the depth of rubble in a fully collapsed drift was estimated to be 8.1 to 13.2 m deep (Section 5.3.2), so the depth of the rubble is larger than the maximum depth that the fuel rods can sustain. These results indicate that exposed fuel assemblies will fail immediately in a fully collapsed drift. A treatment that includes plasticity might predict less severe consequences.

The static loading reflects assumptions or data on the fraction of the drift that is filled with emplaced materials, the dry bulk density of TSw2 tuff, the fractional density of rubble in the drift, and the diameter of waste emplacement drift. It also reflects the approximation of uniform loading by the rubble. However, the result obtained is that all the fuel rods will be crushed. Since failure of all assemblies is the most severe possible consequence, the values of these inputs and the approximation of uniform loading do not affect the results.

7. ATTACHMENTS

Attachment I. Mathcad workbook for calculating the deflection of a span of a W1717WL fuel rod with fixed ends on impact with an unyielding surface.

Attachment II. Tabulation of results on maximum and minimum curvature, as a function of position, of a W1717WL fuel rod with fixed ends on impact with an unyielding surface. See Section 5.2.3 for explanation.

Attachment III. Mathcad workbook to calculate the probability that a W1717WL fuel rod will fail by fracture, as a function of $f = K_{Ic}^2 / v^2$, where K_{Ic} is the fracture toughness and v is the impact speed.

Attachment IV. Tabulation of the probability that a W1717WL fuel rod will fail by fracture, as a function of f. See Section 5.2.5 for explanation.

Attachment V. Mathcad workbook for calculating the seismic risk for failure of a W1717WL fuel rod.

Attachment VI. Mathcad workbook for calculating the height of drift collapse.

Attachment VII. Sketch of waste package for 21 pressurized water reactor assemblies.

Attachment VIII. Document Input Reference Sheets.

Solve the equations of motion for impact of a fuel assembly with an unyielding surface. Consider one fuel rod in a W1717WL assembly. Treat the span between two spacer grids as an elastic beam with fixed ends. See Sections 5.2.1 through 5.2.3.

Define constants to be used in calculation.

$l := 620.52 \cdot mm$ Maximum distance between two spacer grids, from Section 5.1.

$R := \frac{l}{2} \cdot 9.4996 \cdot mm$ Outside radius of cladding, from Section 5.1.

$w := 0.5715 \cdot mm$ Thickness of cladding, from Section 5.1.

$Ri := R - w$ Inside radius of cladding.

$\rho clad := 6520 \cdot \frac{kg}{m^3} \cdot \pi \cdot \left(R^2 - Ri^2\right)$ Linear mass density of clad. Density of zirconium is from Section 5.1.

$\rho fuel := \frac{461.50 \cdot kg \cdot \frac{238.0289 + 2 \cdot 15.9994}{238.0289}}{264 \cdot 3657.6 \cdot mm}$ Linear mass density of fuel. Amount of uranium per assembly (461.50 kg), molar masses of U (238.0289 g/mol) and O (15.9994 g/mol), number of fuel rods per assembly (264), and active length (3657.6 mm) are from Section 5.1.

$Ert := 145.5 \cdot 10^9 \cdot Pa$ Elastic modulus of zirconium at room temperature from Section 5.1.

$\mu := \frac{\rho clad + \rho fuel}{kg \cdot m^{-1}}$ Linear mass density of fuel rod, kg/m.

$k := \frac{\pi \cdot Ert \cdot w \cdot \left(\frac{R + Ri}{2}\right)^3}{N \cdot m^2}$ Stiffness constant for fuel rod, N·m2. The expression for k is per Equation 20.

$L := \frac{l}{m}$ Length of fuel rod span, m.

$n := 16$ Number of links in half of chain. Value was varied per Table 1 in Section 5.2.3.

$m_l := \frac{\mu \cdot L}{2 \cdot n}$ Mass per link, kg.

$\Delta\tau := 0.000002$ Time step, s. Value was varied per Table 1 in Section 5.2.3.

$tmax := round\left(\frac{0.010}{\Delta\tau}, 0\right)$ Number of time steps. The total time of integration, 0.010 s, was determined from preliminary calculations to be be sufficient to consider a half-oscillation of the beam (see plot of qbar below). Ensure that the number of time steps is an integer.

Define functions for setting and handling arrays and functions

If d > 0, create a square matrix in which the d-th superdiagonal contains the elements in vector v. If d < 0, create a square matrix in which the d-th subdiagonal contains the elements in vector v. If d = 0, return diag(v).

$$supdiag(v,d) := \left| \begin{array}{l} last \leftarrow length(v) + |d| - 1 \\ A_{last,last} \leftarrow 0 \\ \text{for } i \in 0..length(v) - 1 \quad \text{if } d \geq 0 \\ \quad A_{i,d+i} \leftarrow v_i \\ \text{for } i \in 0..length(v) - 1 \quad \text{if } d < 0 \\ \quad A_{i-d,i} \leftarrow v_i \\ A \end{array} \right.$$

$$unit(k) := \left| \begin{array}{l} \text{for } i \in 0..k - 1 \\ \quad v_i \leftarrow 1 \\ v \end{array} \right.$$

Create a vector of length k in which every element is a 1.

$$vec(x) := \left| \begin{array}{l} v_0 \leftarrow x \\ v \end{array} \right.$$

Create a vector of length 1 and value x.

$$magsq(v) := v \cdot v$$

Find the square of the magnitude of vector v.

Define initial conditions and Jacobian matrices for equations of motion. Initial condition is a straight beam with velocity −1 m/s. Other impact speeds can be treated by simply scaling the results obtained here.

$v_{init} := -1$ Initial velocity of particles, $m \cdot s^{-1}$.

$i := 0..n - 1$

$q0_i := 0$ Initial positions of particles, m.

$p0_i := v_{init} \cdot m_I$ Initial momenta of particles, $kg \cdot m \cdot s^{-1}$.

$pq0 := stack(p0, q0)$ Initial state of system.

JCy is the Jacobian matrix for C as a function of y ($JCy_{i,j} = \partial C_{i,t} / \partial y_{j,t}$). The expression for JCy is obtained by differentiating Equation 4.

$$JCy := (-2 \cdot identity(n+1) + supdiag(stack(vec(2), unit(n-1)), 1) + supdiag(stack(unit(n-1), vec(2)), -1)) \cdot \frac{4 \cdot n^2}{L^2}$$

Jyq is the Jacobian matrix for y as a function of q ($Jyq_{k,i} = \partial y_{k,t} / \partial q_{i,t}$). The expression for Jyq is obtained by differentiating Equations 9a and 9e. dummy is a vector of zeroes used to pad Jyq. Jyq is not square because y has n + 1 elements and q has only n.

$$dummy_{n-1} := 0$$

$$Jyq := stack\left[dummy^{T}, \sum_{j=0}^{n-1} supdiag\left[2\cdot(-1)^{j}\cdot unit(n-j), -j\right]\right]$$

J is the Jacobian matrix for C as a function of q ($J_{i,j} = \partial C_{i,t} / \partial q_{j,t}$ per Equation 10). To describe the mechanics of the system, we also need Jhat, which is J modified per Equation 12 to reflect the end effects.

$$J := JCy\cdot Jyq$$

$$Jhat := J$$

$$Jhat_{0,i} := \frac{J_{0,i}}{\sqrt{2}}$$

$$Jhat_{n,i} := \frac{J_{n,i}}{\sqrt{2}}$$

$$JTJ := Jhat^{T}\cdot Jhat$$

Calculate Jhat^T·Jhat (once) for use in equations of motion.

Define and solve equations of motion, then save useful results.

Define equations of motion per Equations 16 and 7.

$$dpqdt(t,pq) := \left|\begin{array}{l} p \leftarrow submatrix(pq,0,n-1,0,0) \\ q \leftarrow submatrix(pq,n,2\cdot n-1,0,0) \\ pdot \leftarrow -\frac{k\cdot L}{2\cdot n}\cdot(JTJ\cdot q) \\ qdot \leftarrow \frac{p}{m_l} \\ stack(pdot,qdot) \end{array}\right.$$

Solve equations of motion ...

$$pq := rkfixed(pq0,0,tmax\cdot\Delta\tau,tmax,dpqdt)$$

... and unpack results. Note that pq0 is a column vector with 2n elements, but pq is a matrix with 2n + 1 columns. (Column 0 of pq contains times.)

$$p := submatrix(pq,0,tmax,1,n)^{T}$$

$$q := submatrix(pq,0,tmax,n+1,2\cdot n)^{T}$$

$$t := 0..tmax$$

Plot the average displacement qbar to ensure that the integration has gone long enough.

$$qbar_t := \frac{\Sigma q^{<t>}}{n}$$

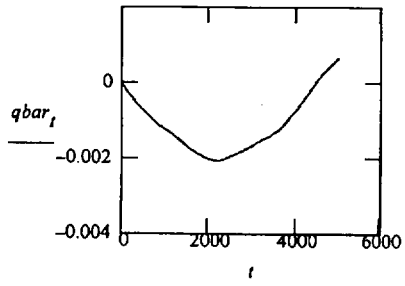

$rebound\_t := for\ i \in 0..length(qbar) - 1$
$\quad return\ i - 1\ if\ qbar_i > 0$

Find the time at which the beam rebounds to zero average displacement.

$rebound\_t = 4471$

$curv := (J \cdot submatrix(q, 0, n - 1, 0, rebound\_t))^T$

Calculate curvature as a function of time and position per Equation 11.

$extmcurv := for\ i \in 0..n$
$\quad mini_i \leftarrow min(curv^{<i>})$
$\quad maxi_i \leftarrow max(curv^{<i>})$
$\quad augment(mini, maxi)$

For each joint, calculate maximum and minimum of curvature with respect to time.

$H_0 := \frac{1}{2 \cdot m_l} \cdot magsq(p^{<0>})$

Calculate the Hamiltonian per Equation 2 at the starting and ending times. At the starting time, the potential energy is zero. At the ending time, using Jhat instead of J cuts the potential energy for each end joint by half, as required by Equation 2.

$H_{rebound\_t} := \frac{1}{2 \cdot m_l} \cdot magsq(p^{<rebound\_t>}) + \frac{k \cdot L}{4 \cdot n} \cdot magsq(Jhat \cdot q^{<rebound\_t>})$

$\frac{H_{rebound\_t}}{H_0} = 0.99431$

$i := 0..n$

$x_i := \frac{i \cdot L}{2 \cdot n}$

Calculate positions of joints.

Save results of calculation for later use. The file beam_curvature.txt will contain n + 1 lines (one for each joint) with 6 numbers in each line. The first number is the number of links, the second is the time step, the third is the ratio of the final value of the Hamiltonian to the initial value, the fourth is the horizontal coordinate of the joint, the fifth is the minimum curvature at the joint, and the sixth is the maximum curvature at the joint.

$results := augment(augment(n \cdot unit(n+1), \Delta t \cdot unit(n+1)), \frac{H_{rebound\_t}}{H_0} \cdot unit(n+1))$

beam curvature.txt

$augment(augment(results, x), extmcurv)$

$tt := floor\left(\frac{rebound\_t}{2}\right)$

Sample display of results for approximately the time of maximum displacement. Display as jointed chain with boxes for masses and lines for beams.

$n = 16$

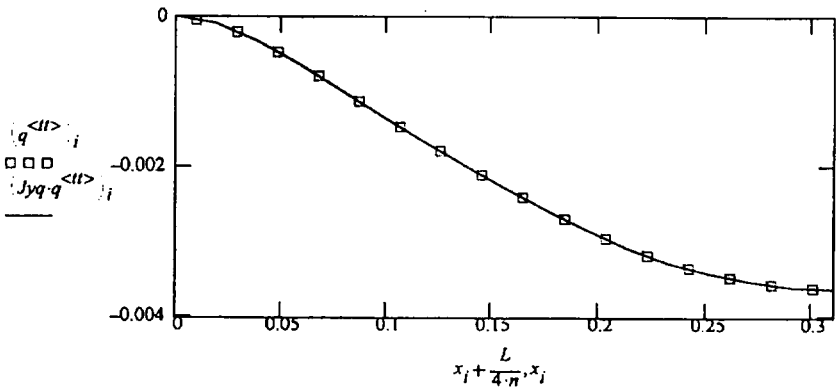

$extmcurv_{0,0} = -0.585$

Test values for verification.

$n = 16$

$extmcurv_{n,1} = 0.384$

```
32 2.5e-007 0.997981075048284 0 -0.67 0.230039881031363
32 2.5e-007 0.997981075048284 0.009695625 -0.457555732694753 0.129889437512867
32 2.5e-007 0.997981075048284 0.01939125 -0.414740446090938 0.131316965352826
32 2.5e-007 0.997981075048284 0.029086875 -0.357234738357511 0.114819912533134
32 2.5e-007 0.997981075048284 0.0387825 -0.341821730072104 0.102980492787743
32 2.5e-007 0.997981075048284 0.048478125 -0.333492425328902 0.112506124503845
32 2.5e-007 0.997981075048284 0.05817375 -0.285739876755307 0.115908754259452
32 2.5e-007 0.997981075048284 0.067869375 -0.268404582925892 0.118533386033098
32 2.5e-007 0.997981075048284 0.077565 -0.250457754600058 0.130079680828809
32 2.5e-007 0.997981075048284 0.087260625 -0.256984983899599 0.137026939392096
32 2.5e-007 0.997981075048284 0.09695625 -0.236129489695657 0.151748876702181
32 2.5e-007 0.997981075048284 0.106651875 -0.247042051366653 0.160054649273505
32 2.5e-007 0.997981075048284 0.1163475 -0.243292317138766 0.159978739119524
32 2.5e-007 0.997981075048284 0.126043125 -0.235253292735255 0.18542368327555
32 2.5e-007 0.997981075048284 0.13573875 -0.235664496891263 0.199033482423054
32 2.5e-007 0.997981075048284 0.145434375 -0.1859475710123 0.186769133846473
32 2.5e-007 0.997981075048284 0.15513 -0.168221447097643 0.22095025442748
32 2.5e-007 0.997981075048284 0.164825625 -0.158423538405517 0.231218764020765
32 2.5e-007 0.997981075048284 0.17452125 -0.138823379967376 0.239597608161749
32 2.5e-007 0.997981075048284 0.184216875 -0.135838343151393 0.242004973425761
32 2.5e-007 0.997981075048284 0.1939125 -0.121078134185425 0.23773890627726
32 2.5e-007 0.997981075048284 0.203608125 -0.135515401466421 0.245669628305003
32 2.5e-007 0.997981075048284 0.21330375 -0.134780160545557 0.25062934520424
32 2.5e-007 0.997981075048284 0.222999375 -0.111468969000862 0.289966104105071
32 2.5e-007 0.997981075048284 0.232695 -0.146587914564067 0.275373715790139
32 2.5e-007 0.997981075048284 0.242390625 -0.131396265886114 0.285153630039662
32 2.5e-007 0.997981075048284 0.25208625 -0.124868350775569 0.299510799118354
32 2.5e-007 0.997981075048284 0.261781875 -0.130046070420757 0.289380314443791
32 2.5e-007 0.997981075048284 0.2714775 -0.10901452334664 0.305980803084372
32 2.5e-007 0.997981075048284 0.281173125 -0.141359407104665 0.332498081967241
32 2.5e-007 0.997981075048284 0.29086875 -0.151484822756155 0.339550883285803
32 2.5e-007 0.997981075048284 0.300564375 -0.166176392481521 0.367151581192616
32 2.5e-007 0.997981075048284 0.31026 -0.22 0.426263991449615
```

Calculate the fragility of a fuel rod for failure by fracture. See Section 5.2.5.

Read and unpack data.

$ntHxnx :=$ C:\..\beam curvature.txt

Read results for curvature of fuel rod as a function of position from previous calculations. Correction has been made in the data file for end effects. x is the distance from the support, Cmin and Cmax are the minimum and maximum curvature, respectively, at each point, divided by impact speed, and n is the number of links.

$x := ntHxnx^{\langle 3 \rangle} \cdot m$

$Cmin := ntHxnx^{\langle 4 \rangle} \cdot \frac{s}{m^2}$

$Cmax := ntHxnx^{\langle 5 \rangle} \cdot \frac{s}{m^2}$

$n := rows(x) - 1$

$vsn := cspline(x, Cmin)$

Define spline interpolants for maximum and minimum curvature of fuel rod.

$vsx := cspline(x, Cmax)$

$C_n(\xi) := interp(vsn, x, Cmin, \xi)$

$C_x(\xi) := interp(vsx, x, Cmax, \xi)$

Set characteristics of fuel rod and flaw distribution.

$N := 60$

Number of flaws from pellet-clad interaction (PCI) in one pressurized water reactor rod, from Section 5.1.

$A_{freq} := 10^{-4}$

Frequency of PCI rod failure, from Section 5.1.

$b := 0.5715 \cdot mm$

Cladding thickness from Section 5.1.

$A_{crit} := 0.28 \cdot b$

Size of critical flaw from Section 5.1.

$$B := \frac{-ln\left[1 - \left(1 - 2 \cdot A_{freq}\right)^{\frac{1}{N}}\right]}{A_{crit}}$$

Parameter for flaw size distribution, per Equation 27.

$B = 7.9 \cdot 10^4 \cdot m^{-1}$

$R := \frac{1}{2} \cdot 9.4996 \cdot mm$

Outside radius of cladding, from Section 5.1.

$Ert := 145.5 \cdot 10^9 \cdot Pa$

Elastic modulus of zirconium at room temperature from Section 5.1.

$l := 620.52 \cdot mm$

Maximum distance between two spacer grids, from Section 5.1.

Calculate fragility.

$$c := \frac{B}{\pi\,(Ert \cdot R)^2}$$

This collection of constants is as defined in Equation 35.

$$expc(x) := \begin{cases} -x - \frac{x^2}{2} - \frac{x^3}{6} - \frac{x^4}{24} & if\ |x| < 0.001 \\ 1 - exp(x) & otherwise \end{cases}$$

The notation for expc is parallel to that for erfc: expc(x) ≡ 1 − exp(x). To provide accurate values of expc for small values of |x|, a series expansion is used (Ref. 23).

Probability of failure for whole rod. See Equations 37 and 38. Per Equation 36, f is $(K_{Ic} / v)^2$ where where K_{Ic} is the mode I fracture toughness and v is the impact speed.

$$P_{frf}(f) := expc\left[\frac{-N}{\pi \cdot l}\cdot\int_{x_0}^{x_n}\int_{0}^{\pi} exp\left(\frac{-c\cdot f}{C_n(\xi)^2\cdot sin(\phi)^2}\right) + exp\left(\frac{-c\cdot f}{C_x(\xi)^2\cdot sin(\phi)^2}\right) d\phi\, d\xi\right]$$

Evaluate P_{frf} for several values of f.

$$ff := (0\ \ 0.1\ \ 0.2\ \ 0.25\ \ 0.3\ \ 0.4\ \ 0.6\ \ 0.8\ \ 1.0\ \ 1.2\ \ 1.5\ \ 2\ \ 2.5\ \ 3\ \ 4\ \ 5\ \ 6\ \ 8\ \ 10\ \ 15\ \ 20)^T \cdot 10^{13} \cdot \left(\frac{Pa^2 \cdot s^2}{m}\right)$$

$$PP := \overrightarrow{P_{frf}(ff)}$$

Plot PP vs. ff to ensure that enough values of ff have been chosen to represent the function.

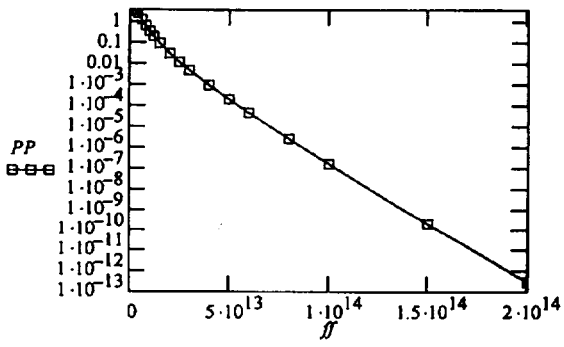

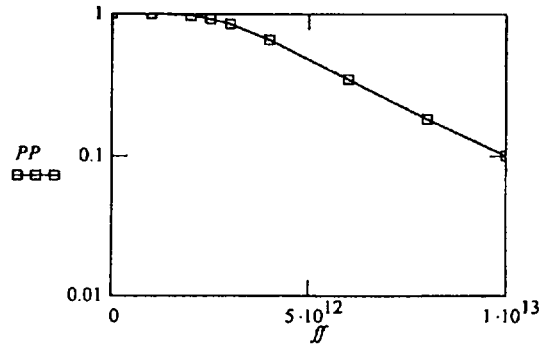

c:\..\fract_curve.txt

$$augment\left(ff \cdot \frac{m}{Pa^2 \cdot s^2}, PP\right)$$

Save results of calculation for later use.

$PP_0 = 1$

Test values for verification.

$PP_8 = 0.0999$

$PP_{15} = 7.832 \cdot 10^{-5}$

```
0 1
1000000000000 0.999798892541993
2000000000000 0.97328170700775
2500000000000 0.92289062739998
3000000000000 0.846098660364586
4000000000000 0.657237488043861
6000000000000 0.346387333405193
8000000000000 0.181377355798378
10000000000000 0.0999448295715587
12000000000000 0.0581513656218038
15000000000000 0.0281133417962594
20000000000000 0.0098238747894327
25000000000000 0.00388964717654394
30000000000000 0.00165972531210323
40000000000000 0.00034347694530506
50000000000000 7.83218669895375e-005
60000000000000 1.89038386962779e-005
80000000000000 1.22247628626893e-006
100000000000000 8.63975771417797e-008
150000000000000 1.4181939908581e-010
200000000000000 2.69610264391946e-013
```

Calculate seismic risk for fuel rod failure by rupture and fracture. See Section 5.2.6.

Define seismic hazard curves and their derivatives.

$$loghah := log\begin{bmatrix} 4.27334\cdot10^{-2} \\ 2.20529\cdot10^{-2} \\ 7.06430\cdot10^{-3} \\ 2.44719\cdot10^{-3} \\ 1.23784\cdot10^{-3} \\ 1.00000\cdot10^{-3} \\ 7.42561\cdot10^{-4} \\ 2.51992\cdot10^{-4} \\ 1.17016\cdot10^{-4} \\ 1.00000\cdot10^{-4} \\ 4.47624\cdot10^{-5} \\ 2.13167\cdot10^{-5} \\ 1.00000\cdot10^{-5} \\ 2.97388\cdot10^{-6} \\ 8.63511\cdot10^{-7} \end{bmatrix} \qquad pgah := \begin{bmatrix} 0.010 \\ 0.020 \\ 0.050 \\ 0.100 \\ 0.150 \\ 0.169 \\ 0.200 \\ 0.350 \\ 0.500 \\ 0.534 \\ 0.750 \\ 1.000 \\ 1.305 \\ 2.000 \\ 3.000 \end{bmatrix} g$$

loghah and loghav are the common logs of the mean seismic hazard (annual probability of exceedance) for peak ground acceleration in the horizontal and vertical directions, respectively. pgah and pgav are the horizontal and vertical peak ground acceleration, respectively. The values given here were taken from Ref. 12.

$$loghav := log\begin{bmatrix} 2.32356\cdot10^{-2} \\ 1.10844\cdot10^{-2} \\ 3.39310\cdot10^{-3} \\ 1.21042\cdot10^{-3} \\ 1.00000\cdot10^{-3} \\ 6.24526\cdot10^{-4} \\ 3.77189\cdot10^{-4} \\ 1.27107\cdot10^{-4} \\ 1.00000\cdot10^{-4} \\ 5.82082\cdot10^{-5} \\ 2.19273\cdot10^{-5} \\ 1.03896\cdot10^{-5} \\ 1.00000\cdot10^{-5} \\ 1.47930\cdot10^{-6} \\ 4.34623\cdot10^{-7} \end{bmatrix} \qquad pgav := \begin{bmatrix} 0.010 \\ 0.020 \\ 0.050 \\ 0.100 \\ 0.112 \\ 0.150 \\ 0.200 \\ 0.350 \\ 0.391 \\ 0.500 \\ 0.750 \\ 1.000 \\ 1.014 \\ 2.000 \\ 3.000 \end{bmatrix} g$$

loghvh and loghvv are the common logs of the seismic hazard (annual probability of exceedance) for peak ground velocity in the horizontal and vertical directions, respectively. pgvh and pgvv are the horizontal and vertical peak ground velocity, respectively. The values given here were taken from Ref. 25.

$$loghvh := log\begin{bmatrix} 8.85219\cdot10^{-2} \\ 5.45892\cdot10^{-2} \\ 3.28919\cdot10^{-2} \\ 1.77397\cdot10^{-2} \\ 6.19274\cdot10^{-3} \\ 2.18808\cdot10^{-3} \\ 1.00000\cdot10^{-3} \\ 6.26181\cdot10^{-4} \\ 2.78161\cdot10^{-4} \\ 1.00000\cdot10^{-4} \\ 9.30240\cdot10^{-5} \\ 1.83594\cdot10^{-5} \\ 1.00000\cdot10^{-5} \\ 3.07391\cdot10^{-6} \\ 2.28195\cdot10^{-7} \end{bmatrix} \qquad pgvh := \begin{bmatrix} 0.200 \\ 0.500 \\ 1.000 \\ 2.000 \\ 5.000 \\ 10.000 \\ 15.431 \\ 20.000 \\ 30.000 \\ 48.342 \\ 50.000 \\ 100.000 \\ 126.571 \\ 200.000 \\ 500.000 \end{bmatrix} \frac{cm}{s}$$

$$loghvv := log\begin{bmatrix} 5.99752\cdot10^{-2} \\ 3.12208\cdot10^{-2} \\ 1.66747\cdot10^{-2} \\ 7.67901\cdot10^{-3} \\ 2.06935\cdot10^{-3} \\ 1.00000\cdot10^{-3} \\ 6.22514\cdot10^{-4} \\ 1.59968\cdot10^{-4} \\ 1.00000\cdot10^{-4} \\ 6.69268\cdot10^{-5} \\ 2.04219\cdot10^{-5} \\ 1.00000\cdot10^{-5} \\ 3.47949\cdot10^{-6} \\ 4.99996\cdot10^{-7} \\ 2.81242\cdot10^{-8} \end{bmatrix} \qquad pgvv := \begin{bmatrix} 0.200 \\ 0.500 \\ 1.000 \\ 2.000 \\ 5.000 \\ 7.607 \\ 10.000 \\ 20.000 \\ 24.887 \\ 30.000 \\ 50.000 \\ 66.134 \\ 100.000 \\ 200.000 \\ 500.000 \end{bmatrix} \frac{cm}{s}$$

$$linderiv(vx, vy, x) := \begin{| imax \leftarrow length(vx) - 1 \\ i \leftarrow 1 \\ while\ i < imax \\ \quad \left| return\ \frac{vy_i - vy_{i-1}}{vx_i - vx_{i-1}}\ if\ x \le vx_i \right. \\ \quad \left| i \leftarrow i + 1 \right. \\ \frac{vy_i - vy_{i-1}}{vx_i - vx_{i-1}} \end|$$

Derivative of a linear interpolant.

$hah(a) := 10^{(linterp(pgah, loghah, a)) \cdot yr^{-1}}$

$hav(a) := 10^{(linterp(pgav, loghav, a)) \cdot yr^{-1}}$

$hvh(v) := 10^{(linterp(pgvh, loghvh, v)) \cdot yr^{-1}}$

$hvv(v) := 10^{(linterp(pgvv, loghvv, v)) \cdot yr^{-1}}$

Interpolate linearly to find the seismic hazards (annual probability of exceedance) for horizontal acceleration, vertical acceleration, horizontal velocity, and vertical velocity, respectively.

$dhah\_da(a) := ln(10) \cdot hah(a) \cdot linderiv(pgah, loghah, a)$

$dhav\_da(a) := ln(10) \cdot hav(a) \cdot linderiv(pgav, loghav, a)$

$dhvh\_dv(v) := ln(10) \cdot hvh(v) \cdot linderiv(pgvh, loghvh, v)$

$dhvv\_dv(v) := ln(10) \cdot hvv(v) \cdot linderiv(pgvv, loghvv, v)$

Derivative of seismic hazard with respect to peak ground acceleration or peak ground velocity, as appropriate.

Determine largest accelerations and velocities that need to be considered (those with annual probabilities of exceedance are less than 10^{-8} yr^{-1}). First, provide initial guesses for root-finder.

$ahmax := 40 \cdot m \cdot s^{-2}$ $avmax := 40 \cdot m \cdot s^{-2}$ $vhmax := 6 \cdot m \cdot s^{-1}$ $vvmax := 6 \cdot m \cdot s^{-1}$

$ahmax := root(hah(ahmax) \cdot 10^8 \cdot yr - 1, ahmax)$

$avmax := root(hav(avmax) \cdot 10^8 \cdot yr - 1, avmax)$

$vhmax := root(hvh(vhmax) \cdot 10^8 \cdot yr - 1, vhmax)$

$vvmax := root(hvv(vvmax) \cdot 10^8 \cdot yr - 1, vvmax)$

Then solve for correct values.

Finally, verify that the values are correct.

$hah(ahmax) = 1.0 \cdot 10^{-8} \cdot yr^{-1}$ $hav(avmax) = 1.0 \cdot 10^{-8} \cdot yr^{-1}$ $hvh(vhmax) = 1.0 \cdot 10^{-8} \cdot yr^{-1}$ $hvv(vvmax) = 1.0 \cdot 10^{-8} \cdot yr^{-1}$

Define fragility for rupture and calculate risk.

$gap := 226.4 \cdot mm - 214.0204 \cdot mm$

$gap = 0.0124\ \text{m}$

gap is the difference between the width of a fuel basket tube (226.4 mm) (from Section 5.1) and the width of a spacer grid (214.0204 mm) (from Section 5.1).

$Ert := 145.5 \cdot 10^9 \cdot Pa$

Elastic modulus of zirconium at room temperature from Section 5.1.

$\sigma y := 1.55 \cdot 10^9 \cdot Pa$

Yield strength of irradiated cladding from Section 5.1.

$R := \frac{1}{2} \cdot 9.4996 \cdot mm$

Outside radius of cladding, from Section 5.1.

$$vrup := \frac{\sigma y}{0.67 \cdot \frac{s}{m^2} \cdot Ert \cdot R}$$

$vrup = 3.347\ \text{m} \cdot \text{s}^{-1}$

Minimum speed of impact for rod failure by rupture. For impact at speed v, maximum curvature of a fuel rod is v·0.67 s/m^2. Elastic strain at yield point is σy/Ert. The extreme fiber strain is the curvature times R. See Equation 23.

$$P_{frr}(v) := \Phi\left(\frac{v}{vrup} - 1\right)$$

Probability of rod failure by rupture (fragility) is 0 for v < vrup and 1 otherwise. See Equation 23.

$$R_{2rh} := \int_{0 \cdot m \cdot s^{-2}}^{ahmax} -dhah\_da(a) \cdot P_{frr}\left(\sqrt{2 \cdot a \cdot gap}\right) da$$

$$R_{2rv} := \int_{0 \cdot m \cdot s^{-2}}^{avmax} -dhav\_da(a) \cdot P_{frr}\left(\sqrt{2 \cdot a \cdot gap}\right) da$$

Rate at which fuel rods break by rupture (risk), as limited by the gap between the fuel assembly and the fuel basket tube and by the peak horizontal and vertical ground accelerations, respectively. These risks apply if displacements are limited by fuel basket geometry. $(2a \cdot gap)^{1/2}$ is speed that would be attained if an acceleration of a is sustained over a distance of gap. See Equations 22 and 39. Here and below, the subscripts to R indicate the scenario number (1 or 2), the failure mechanism (r for rupture or f for fracture), and the direction of ground motion (h for horizontal or v for vertical), respectively.

$$R_{1rh} := \int_{vrup}^{vhmax} -dhvh\_dv(v) \cdot P_{frr}(v)\, dv$$

$$R_{1rv} := \int_{vrup}^{vvmax} -dhvv\_dv(v) \cdot P_{frr}(v)\, dv$$

Rate at which fuel rods break by rupture (risk), as limited by the horizontal and vertical peak ground velocities, respectively. These risks apply if large displacements are possible. See Equation 39.

$\sqrt{2 \cdot ahmax \cdot gap} = 1.266\ \text{m} \cdot \text{s}^{-1}$

Note that the maximum possible velocity is smaller than vrup.

Define fragility for fracture and calculate risk.

$KP :=$

C:\..\fract_curve.txt

Read data for fracture of fuel rods. lnPfr is the natural logarithm of the probability of rod failure for a given impact. Kv is $(K_{Ic} / v)^2$ where K_{Ic} is the mode I fracture toughness and v is the impact speed. See Attachment III, page III-2.

$Kv := KP^{\langle 0 \rangle} \cdot \frac{Pa^2 \cdot s^2}{m}$

$Pfr := KP^{\langle 1 \rangle}$

$lnPfr := ln(Pfr)$

$P_{frf}(f) := exp(linterp(Kv, lnPfr, f))$

Define a function for the probability of rod failure by fracture. f is the current value of $(K_{Ic} / v)^2$. Pfrf is the probability of rod failure. See Attachment III, page III-2.

$Klc := 17 \cdot 10^6 \cdot Pa \cdot m^{\frac{1}{2}}$

Fracture toughness from Section 5.1. Value is for 5th percentile.

Rate at which fuel rods break by fracture (risk), as limited by the gap between the fuel assembly and the fuel basket tube and by the peak horizontal and vertical ground accelerations, respectively. These risks apply if displacements are limited by fuel basket geometry. The factor $1 - P_{frr}((2a \cdot gap)^{1/2})$ applies because fracture is irrelevant if a rod has already failed by rupture. See Equations 22 and 39.

$$R_{2fh} := \int_{0 \cdot m \cdot s^{-2}}^{ahmax} -dhah\_da(a) \cdot P_{frf}\left(\frac{Klc^2}{2 \cdot a \cdot gap}\right) \cdot \left(1 - P_{frr}\left(\sqrt{2 \cdot a \cdot gap}\right)\right) da$$

$$R_{2fv} := \int_{0 \cdot m \cdot s^{-2}}^{avmax} -dhav\_da(a) \cdot P_{frf}\left(\frac{Klc^2}{2 \cdot a \cdot gap}\right) \cdot \left(1 - P_{frr}\left(\sqrt{2 \cdot a \cdot gap}\right)\right) da$$

$P_{frf}\left(\frac{Klc^2}{2 \cdot ahmax \cdot gap}\right) = 3.2 \cdot 10^{-12}$

Note that the fragility is extremely small even for the largest possible velocity.

Rate at which fuel rods break by fracture (risk), as limited by the peak ground velocity. These risks apply if large displacements are possible. The factor $1 - P_{frr}(v)$ applies because fracture is irrelevant if a rod has already failed by rupture. See Equation 39.

$$R_{1fh} := \int_{0 \cdot m \cdot s^{-1}}^{vhmax} -dhvh\_dv(v) \cdot P_{frf}\left[\left(\frac{KIc}{v}\right)^2\right] \cdot \left(1 - P_{frr}(v)\right) dv$$

$$R_{1fv} := \int_{0 \cdot m \cdot s^{-1}}^{vvmax} -dhvv\_dv(v) \cdot P_{frf}\left[\left(\frac{KIc}{v}\right)^2\right] \cdot \left(1 - P_{frr}(v)\right) dv$$

Summary of risks for all combinations of scenario, failure mechanism, and direction of ground motion.

$R_{1rh} = 9.5 \cdot 10^{-7} \cdot yr^{-1}$

$R_{1rv} = 1.3 \cdot 10^{-7} \cdot yr^{-1}$

$R_{1fh} = 7.7 \cdot 10^{-10} \cdot yr^{-1}$

$R_{1fv} = 1.6 \cdot 10^{-10} \cdot yr^{-1}$

$R_{2rh} = 0.0 \cdot yr^{-1}$

$R_{2rv} = 0.0 \cdot yr^{-1}$

$R_{2fh} = 1.5 \cdot 10^{-20} \cdot yr^{-1}$

$R_{2fv} = 1.7 \cdot 10^{-21} \cdot yr^{-1}$

$R_{1rh} + R_{1rv} + R_{1fh} + R_{1fv} + R_{2rh} + R_{2rv} + R_{2fv} + R_{2rv} = 1.1 \cdot 10^{-6} \cdot yr^{-1}$

Calculate height of rubble pack for a fully collapsed drift. See see Section 5.3.2.

The configuration of a fully collapsed circular drift is not known. This attachment considers three simple geometries in an attempt to describe the configuration. The as-built configuration is an empty cylindrical drift with radius 1, surrounded by fully dense rock. The collapsed configuration is a drift (original drift plus additional volume that was originally occupied by host rock) that is completely filled by rubble with a fractional density of ψ ($0 < \psi < 1$). Extent of collapse is limited by conservation of matter.

The three geometries are as follows: (1) Rectangular. The original surface of the circular drift is intact up to the springline. The cross section above the original springline is a rectangle. (2) Elliptical. The original surface of the circular drift is intact up to the springline. The cross section above the original springline is half of an ellipse. (3) Triangular. The original surface of the circular drift is intact to an elevation somewhat above the springline. The cross section above that elevation is an isosceles triangle. The legs of the triangle are tangent to the original surface of the drift. Sketches of the three cross sections are shown below.

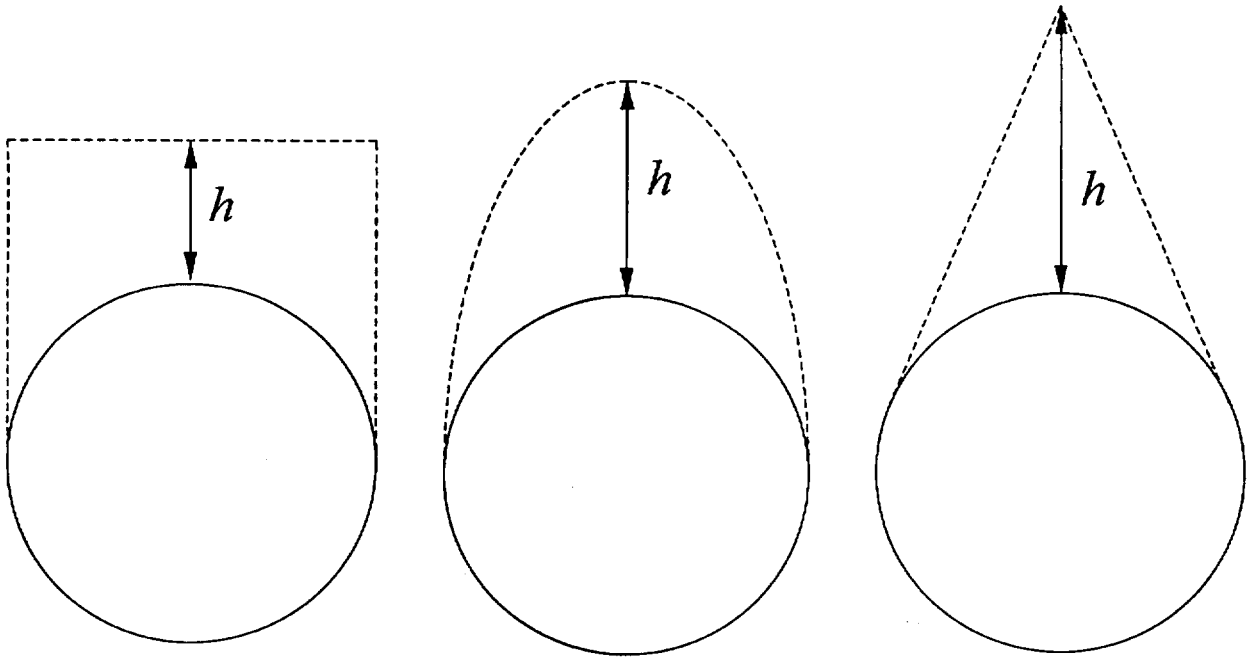

$\psi := 0.6$ Fractional density of the rubble (from Section 5.1).

$f := 0.5$ Fraction of the original drift cross section that is filled (e.g., with invert materials, waste packages, etc.) before collapse occurs (from Section 3).

Case 1. In the symbolic equations below, the left hand side is the area of material in the collapsed drift and the right hand side is the area from which the material came. The expressions are from standard mensuration formulas for circles and rectangles.

$$\psi \cdot \left[2 \cdot (h + 1) + \frac{\pi}{2} - \pi \cdot f \right] = 2 \cdot (h + 1) - \frac{\pi}{2}$$

Express conservation of matter (per Equation 45) for rectangular geometry.

$$\frac{-2 \cdot \psi + \frac{1}{2} \cdot \psi \cdot \pi - \psi \cdot \pi \cdot f - 2 + \frac{1}{2} \cdot \pi}{2 \cdot \psi - 2}$$

Solve for h ...

$$h1 := \frac{1}{4}\cdot\frac{-4\cdot\psi - \psi\cdot\pi + 2\cdot\psi\cdot\pi\cdot f + 4 - \pi}{\psi - 1}$$

and simplify.

Case 2. The symbolic equation below uses the standard mensuration formula for the area of an ellipse: πab, where a and b are the semiaxis lengths.

$$\psi\cdot\left[\frac{\pi}{2}\cdot(h+2) - \pi\cdot f\right] = \frac{\pi}{2}\cdot h$$

Express conservation of matter (per Equation 45) for elliptical geometry.

$$\frac{-\left(\psi\cdot\pi - \psi\cdot\pi\cdot f\right)}{\frac{1}{2}\cdot\psi\cdot\pi - \frac{1}{2}\cdot\pi}$$

Solve for h ...

$$h2 := 2\cdot\psi\cdot\frac{(-1+f)}{\psi - 1}$$

and simplify.

Case 3. The symbolic equation below uses standard mensuration formulas for triangles and sectors of circles. The cross section of the collapsed drift is dissected into a sector of a circle plus two congruent right triangles. The vertices of one triangle are at the center of the original drift, the apex of the collapsed region, and the point of tangency between the surface of the original drift and the surface of the collapsed region. Each triangle has a hypotenuse length of 1 + h and leg lengths of 1 and $[(1 + h)^2 - 1]^{1/2} = (h^2 + 2h)^{1/2}$. The region of overlap between one triangle and the original circular drift is a sector with a central angle of acos(1 / (h + 1)).

Express conservation of matter (per Equation 45) for triangular geometry.

$$\psi\cdot\left(\sqrt{h^2+2\cdot h} - acos\left(\frac{1}{h+1}\right) + \pi - \pi\cdot f\right) = \sqrt{h^2+2\cdot h} - acos\left(\frac{1}{h+1}\right)$$

No analytic solution to the equation was found, so the equation was solved numerically. Here is the initial guess for the root-finder.

$$h := 5$$

$$h3 := root\left[\psi\cdot\left(\sqrt{h^2+2\cdot h} - acos\left(\frac{1}{h+1}\right) + \pi - \pi\cdot f\right) - \left(\sqrt{h^2+2\cdot h} - acos\left(\frac{1}{h+1}\right)\right), h\right]$$

$$hh := (h1 \quad h2 \quad h3)$$

Collect and display results.

$$hh = (0.9635 \quad 1.5000 \quad 2.7947)$$

$$r := \frac{5.5\cdot m}{2}$$

Actual drift radius (from Section 5.1).

$$(hh + 2)\cdot r = (8.1 \quad 9.6 \quad 13.2)\ \text{m}$$

Maximum depth of rubble measured from invert of drift.

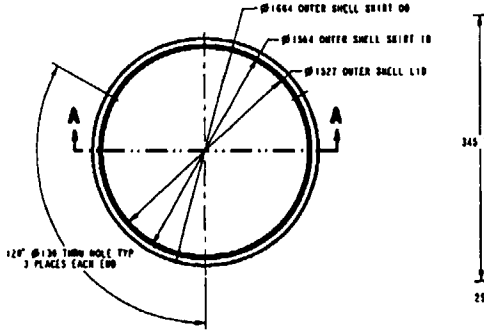

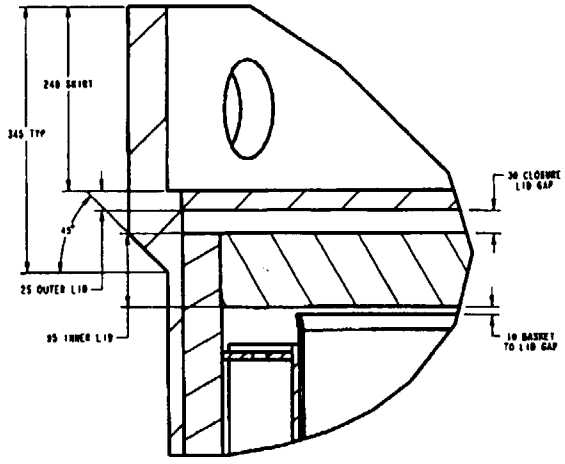

DETAIL A

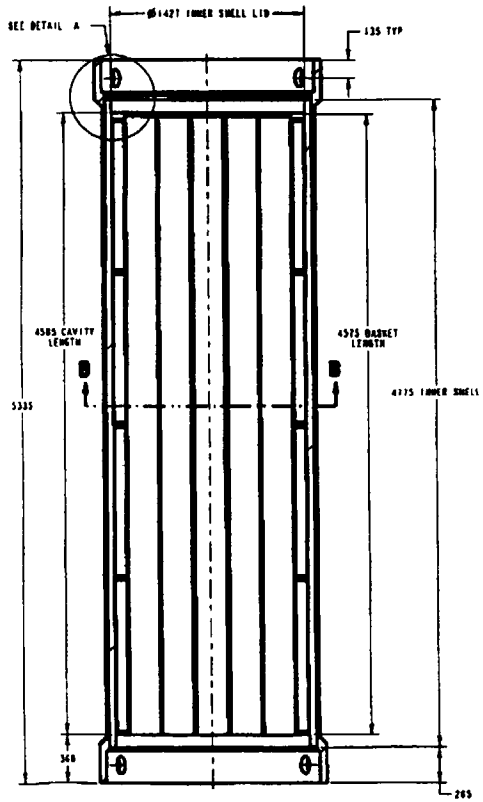

SECTION A-A

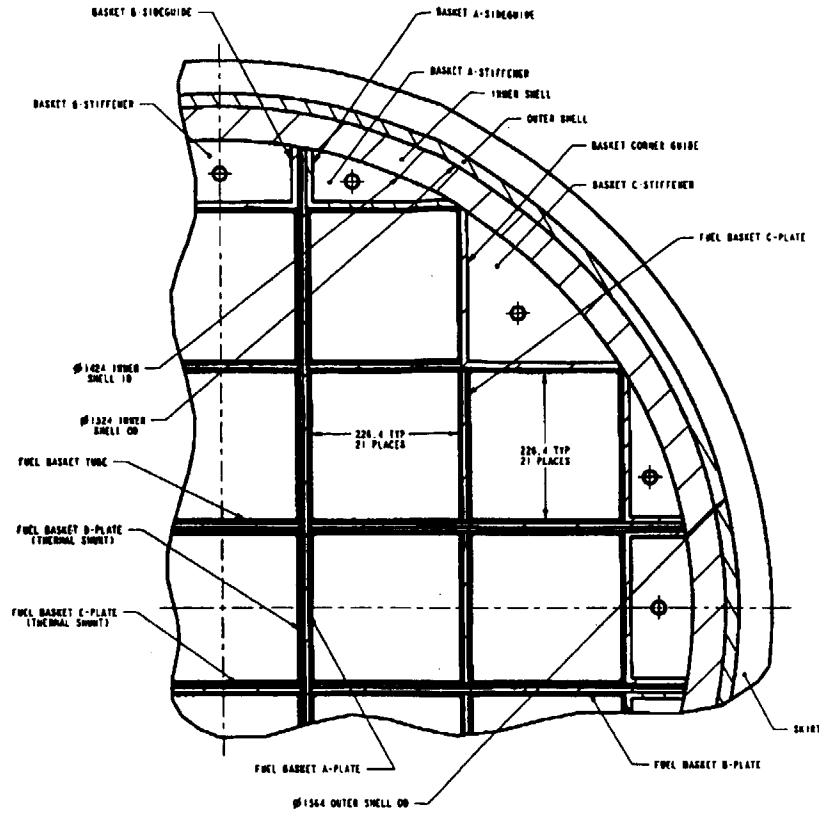

SECTION B-B

COMPONENT NAME	MATERIAL	THICKNESS	MASS (KG)	QTY REQ
BASKET A-SIDEGUIDE	SA-516 G02700	10	27	32
BASKET A-STIFFENER	SA-516 G02700	10	0.72	64
BASKET B-SIDEGUIDE	SA-516 G02700	10	36	16
BASKET B-STIFFENER	SA-516 G02700	10	1.9	32
BASKET C-STIFFENER	SA-516 G02700	10	2.3	32
BASKET CORNER GUIDE	SA-516 G02700	10	42	16
FUEL BASKET A-PLATE	NEUTRONIT A 978	7	85	8
FUEL BASKET B-PLATE	NEUTRONIT A 978	7	85	8
FUEL BASKET C-PLATE	NEUTRONIT A 978	7	44	16
FUEL BASKET D-PLATE	SB-209 A96061 T4	5	21	8
FUEL BASKET E-PLATE	SB-209 A96061 T4	5	21	8
FUEL BASKET TUBE	SA-516 G02700	5	164	21
INNER SHELL	SA-240 (316NG)	50	8612	1
INNER SHELL LID	SA-240 (316NG)	95	1212	2
OUTER SHELL	SB-575 N06022	20	5464	1
OUTER SHELL LID	SB-575 N06022	25	388	2
WASTE PACKAGE ASSEMBLY	-	-	25619	1
PWR FUEL ASSEMBLY	-	-	773.4*	21
BP ASSEMBLY WITH SHF	-	-	41860	1

* CRWMS M&O 1997. WASTE CONTAINER CAVITY SIZE DETERMINATION. SBAA00000-01717-0200-00026 REV 00. LAS VEGAS, NV: CRWMS M&O. ACC: MOL.19980106.0061

REVISION 03	
ITEM NUMBER	REMARK
1	ϕ130 LIFTING FEATURE WAS ϕ125 ON TOP VIEW
2	5464 OUTER SHELL MASS WAS 5445 ON DATA TABLE
3	25619 WASTE PACKAGE ASSEMBLY MASS WAS 25690 ON DATA TABLE
4	41860 WP ASSEMBLY WITH SHF WAS 41841 ON DATA TABLE
5	5335 WASTE PACKAGE ASSEMBLY LENGTH WAS 5325 ON SECTION A-A
6	240 SKIRT LENGTH WAS 235 ON DETAIL A
7	345 FLARED SKIRT LENGTH WAS 340 ON DETAIL A
8	265 SKIRT END TO LID LENGTH WAS 260 ON SECTION A-A
9	360 SKIRT END TO INNER LID LENGTH WAS 355 ON SECTION A-A

"FOR INFORMATION ONLY"

SINGLE CRM 21-PWR WASTE PACKAGE

SKETCH NUMBER: SK-0132 REV 03

SKETCHED BY: BRYAN HARKINS 16 July 99 SMB 07/16/99 J.CTP 7.16.99

DATE: 07/16/99

FILE: /home/pro_library/checkout/sketches/21pwr_home/sk-0132_rev03/sk-0132_rev03.dwg

UNITS: mm
DO NOT SCALE FROM SKETCH

OFFICE OF CIVILIAN RADIOACTIVE WASTE MANAGEMENT
DOCUMENT INPUT REFERENCE SHEET

1. Document Identifier No./Rev.:	Change:	Title:
CAL-EBS-MD-000001 REV 00	N/A	Breakage of Commercial Spent Nuclear Fuel Cladding by Mechanical Loading

Input Document							8. TBV Due To		
	2. Technical Product Input Source Title and Identifier(s) with Version	3. Section	4. Input Status	5. Section Used In	6. Input Description	7. TBV/TBD Priority	Unqual.	From Uncontrolled Source	Un-confirmed
2a 1	Doering, T.W. 1999. "Assistant Manager, Office of Project Execution (AMOPE) Concurrence of Rationale for Identifying Technical Information as Accepted Data." Letter from T.W. Doering (CRWMS M&O) to R.E. Spence (DOE/YMSCO), August 20, 1999, LV.WP.TWD.08/99-131. ACC: MOL.19990914.0204.	entire	N/A Used as a reference only.	5.1	request for approval of accepted data	N/A	N/A	N/A	N/A
2	Mellington, S.P. 1999. "Office of Project Execution (OPE) Approval of LV.WP.TWD.08/99-131 as Accepted Data." Letter from S.P. Mellington (DOE/YMSCO) to T.W. Doering (CRWMS M&O), September 29, 1999. ACC: MOL.19990927.0472.	entire	N/A Used as a reference only.	5.1	approval of accepted data	N/A	N/A	N/A	N/A
3	Lide, D.R., ed. 1995. *CRC Handbook of Chemistry and Physics, 76th Edition 1995-1996.* Boca Raton, Florida: CRC Press. TIC: 216194.	inside front cover	N/A Data are established fact.	5.1, Att. I	(1) molar mass of natural uranium, (2) molar mass of oxygen	N/A	N/A	N/A	N/A

OFFICE OF CIVILIAN RADIOACTIVE WASTE MANAGEMENT
DOCUMENT INPUT REFERENCE SHEET

1. Document Identifier No./Rev.:	Change:	Title:
CAL-EBS-MD-000001 REV 00	N/A	Breakage of Commercial Spent Nuclear Fuel Cladding by Mechanical Loading

Input Document			4. Input Status	5. Section Used in	6. Input Description	7. TBV/TBD Priority	8. TBV Due To		
	2. Technical Product Input Source Title and Identifier(s) with Version	3. Section					Unqual.	From Uncontrolled Source	Un-confirmed
2a 4	Lide, D.R., ed. 1995. *CRC Handbook of Chemistry and Physics, 76th Edition 1995-1996.* Boca Raton, Florida: CRC Press. TIC: 216194.	page 4-98	N/A Data are established fact.	5.1, Att. I	density of zirconium at room temperature	N/A	N/A	N/A	N/A
5	NUREG/CR-1729, Volume 1. 1981. *Evaluating Strength and Ductility of Irradiated Zircaloy, Task 5. Experimental Data Final Report.* Washington, D.C.: U.S. Nuclear Regulatory Commission. TIC: 238074. INITIAL USE	Table 34, line 1; table 35, line 5	TBV-3480	5.1, 5.3.1, Att. I, Att. III, Att. V	(1) elastic modulus of irradiated Zircaloy cladding in bending at room temperature, (2) yield strength (0.02% maximum fiber strain) of irradiated Zircaloy cladding in bending at room temperature	2	N/A	✓	N/A
6	Parker, S.P., ed. 1983. *McGraw-Hill Dictionary of Scientific and Technical Terms, Third Edition.* New York, New York: McGraw-Hill Book Company. TIC: 220032.	page 722	N/A Data are established fact.	5.1, 5.2.1	Hamilton's equations of motion	N/A	N/A	N/A	N/A

OFFICE OF CIVILIAN RADIOACTIVE WASTE MANAGEMENT
DOCUMENT INPUT REFERENCE SHEET

1. Document Identifier No./Rev.:	Change:	Title:
CAL-EBS-MD-000001 REV 00	N/A	Breakage of Commercial Spent Nuclear Fuel Cladding by Mechanical Loading

Input Document			4. Input Status	5. Section Used in	6. Input Description	7. TBV/TBD Priority	8. TBV Due To		
	2. Technical Product Input Source Title and Identifier(s) with Version	3. Section					Unqual.	From Uncontrolled Source	Un-confirmed
2a 7	Sanders, T.L.; Seager, K.D.; Rashid, Y.R.; Barrett, P.R.; Malinauskas, A.P.; Einziger, R.E.; Jordan, H.; Duffey, T.A.; Sutherland, S.H.; and Reardon, P.C. 1992. *A Method for Determining the Spent-Fuel Contribution to Transport Cask Containment Requirements.* SAND90-2406. Albuquerque, New Mexico: Sandia National Laboratories. TIC: 232162.	page III-58, Figure III-32	N/A Data do not affect the results.	5.1, Att. V	fracture toughness of irradiated cladding, 5th percentile value	N/A	N/A	N/A	N/A
8	Sanders, T.L.; Seager, K.D.; Rashid, Y.R.; Barrett, P.R.; Malinauskas, A.P.; Einziger, R.E.; Jordan, H.; Duffey, T.A.; Sutherland, S.H.; and Reardon, P.C. 1992. *A Method for Determining the Spent-Fuel Contribution to Transport Cask Containment Requirements.* SAND90-2406. Albuquerque, New Mexico: Sandia National Laboratories. TIC: 232162.	page I-55	N/A Data do not affect the results.	5.1, 5.2.5, Att. III	number of pellet-clad interaction flaws per pressurized water reactor fuel rod	N/A	N/A	N/A	N/A
9	Sanders, T.L.; Seager, K.D.; Rashid, Y.R.; Barrett, P.R.; Malinauskas, A.P.; Einziger, R.E.; Jordan, H.; Duffey, T.A.; Sutherland, S.H.; and Reardon, P.C. 1992. *A Method for Determining the Spent-Fuel Contribution to Transport Cask Containment Requirements.* SAND90-2406. Albuquerque, New Mexico: Sandia National Laboratories. TIC: 232162.	page III-58	N/A Data do not affect the results.	5.1, 5.2.5, Att. III	frequency of rod failure by pellet-clad interaction	N/A	N/A	N/A	N/A

OFFICE OF CIVILIAN RADIOACTIVE WASTE MANAGEMENT
DOCUMENT INPUT REFERENCE SHEET

1. Document Identifier No./Rev.:	Change:	Title:
CAL-EBS-MD-000001 REV 00	N/A	Breakage of Commercial Spent Nuclear Fuel Cladding by Mechanical Loading

Input Document			4. Input Status	5. Section Used in	6. Input Description	7. TBV/TBD Priority	8. TBV Due To		
	2. Technical Product Input Source Title and Identifier(s) with Version	3. Section					Unqual.	From Uncontrolled Source	Un-confirmed
2a 10	Sanders, T.L.; Seager, K.D.; Rashid, Y.R.; Barrett, P.R.; Malinauskas, A.P.; Einziger, R.E.; Jordan, H.; Duffey, T.A.; Sutherland, S.H.; and Reardon, P.C. 1992. *A Method for Determining the Spent-Fuel Contribution to Transport Cask Containment Requirements.* SAND90-2406. Albuquerque, New Mexico: Sandia National Laboratories. TIC: 232162.	page I-52	N/A Data do not affect the results.	5.1, 5.2.5, Att. III	size of critical flaw as a fraction of cladding thickness for fuel rod failure by pellet-clad interaction	N/A	N/A	N/A	N/A
11	CRWMS M&O 1998. *Summary Report of Commercial Reactor Criticality Data for Sequoyah Unit 2.* B00000000-01717-5705-00064 REV 01. Las Vegas, Nevada: CRWMS M&O. ACC: MOL.19980716.0015.	Table 2-2 (items 1, 2), Figure 2-3 (item 3), Figure 2-4 (items 4, 5), Table 3-1, line for fresh fuel batch 5A (items 6, 7, 8)	N/A Data are accepted.	5.1, 5.2.5, 5.3.1, Att. I, Att. III, Att. V	characteristics of W1717WL fuel assembly: (1) number of fuel rods per assembly, (2) rod pitch, (3) width of an assembly, (4) active length, (5) maximum distance between two spacer grids, (6) mass of uranium per assembly, (7) outside diameter of cladding, (8) thickness of cladding	N/A	N/A	N/A	N/A
12	CRWMS M&O 1999. *Seismic Ground Motion Hazard Inputs.* Input Transmittal WP-NEP-99309.T. Las Vegas, Nevada: CRWMS M&O. ACC: MOL.19991005.0147. INITIAL USE	page A1-3 (item 1) page A1-5 (item 2)	TBV-3481	5.1, 5.2.6, Att. V	(1) mean seismic hazard for horizontal peak ground acceleration, (2) mean seismic hazard for vertical peak ground acceleration	2	✓	N/A	N/A

OFFICE OF CIVILIAN RADIOACTIVE WASTE MANAGEMENT
DOCUMENT INPUT REFERENCE SHEET

1. Document Identifier No./Rev.:	Change:	Title:
CAL-EBS-MD-000001 REV 00	N/A	Breakage of Commercial Spent Nuclear Fuel Cladding by Mechanical Loading

Input Document			4. Input Status	5. Section Used in	6. Input Description	7. TBV/TBD Priority	8. TBV Due To		
	2. Technical Product Input Source Title and Identifier(s) with Version	3. Section					Unqual.	From Uncontrolled Source	Un-confirmed
2a 13	CRWMS M&O 1998. *Rock Geomechanical Properties.* Las Vegas, Nevada: CRWMS M&O. ACC: MOL.19981124.0096.	Table 1, TSw2, all holes	N/A Data do not affect the results.	5.1, 5.3.1	dry bulk density of TSw2 tuff	N/A	N/A	N/A	N/A
14	Brown, R.L. and Richards, J.C. 1970. "Chapter 2, Packings." *Principles of Powder Mechanics.* 13-19, 22. Oxford, England: Pergamon Press. TIC: 239150.	Table 2.2	N/A Data do not affect the results.	5.1, 5.3.1, Att. VI	fractional solids content of graded granular powder	N/A	N/A	N/A	N/A
15	CRWMS M&O 1997. *Typical Emplacement Drift and Ventilation Raise Sections, Elevations.* BCAA00000-01717-2700-81035 REV 00. Las Vegas, Nevada: CRWMS M&O. ACC: MOL.19971215.0955.	Zone B-7	N/A Data do not affect the results.	5.1, Att. VI	diameter of waste emplacement drift	N/A	N/A	N/A	N/A

OFFICE OF CIVILIAN RADIOACTIVE WASTE MANAGEMENT
DOCUMENT INPUT REFERENCE SHEET

1. Document Identifier No./Rev.:	Change:	Title:
CAL-EBS-MD-000001 REV 00	N/A	Breakage of Commercial Spent Nuclear Fuel Cladding by Mechanical Loading

Input Document			4. Input Status	5. Section Used in	6. Input Description	7. TBV/TBD Priority	8. TBV Due To		
	2. Technical Product Input Source Title and Identifier(s) with Version	3. Section					Unqual.	From Uncontrolled Source	Un-confirmed
2a 16	DOE 1996. *Spent Nuclear Fuel Discharges from U.S. Reactors 1994.* SR/CNEAF/96-01. Washington, D.C.: U.S. Department of Energy, Energy Information Administration. TIC: 232923.	Table B-8	N/A Used as a reference only.	5, 5.1	number of pressurized water reactor fuel assemblies discharged, by type	N/A	N/A	N/A	N/A
17	DOE 1996. *Spent Nuclear Fuel Discharges from U.S. Reactors 1994.* SR/CNEAF/96-01. Washington, D.C.: U.S. Department of Energy, Energy Information Administration. TIC: 232923.	Table B-4	N/A Used as a reference only.	5, 5.1	descriptions of fuel assembly types	N/A	N/A	N/A	N/A
18	Sanders, T.L.; Seager, K.D.; Rashid, Y.R.; Barrett, P.R.; Malinauskas, A.P.; Einziger, R.E.; Jordan, H.; Duffey, T.A.; Sutherland, S.H.; and Reardon, P.C. 1992. *A Method for Determining the Spent-Fuel Contribution to Transport Cask Containment Requirements.* SAND90-2406. Albuquerque, New Mexico: Sandia National Laboratories. TIC: 232162.	page III-68	N/A Used as a reference only.	5.1, 5.2.5	equations for stress intensity factor for a surface crack in a tube subjected to bending loads	N/A	N/A	N/A	N/A

OFFICE OF CIVILIAN RADIOACTIVE WASTE MANAGEMENT
DOCUMENT INPUT REFERENCE SHEET

1. Document Identifier No./Rev.:	Change:	Title:
CAL-EBS-MD-000001 REV 00	N/A	Breakage of Commercial Spent Nuclear Fuel Cladding by Mechanical Loading

Input Document			4. Input Status	5. Section Used in	6. Input Description	7. TBV/TBD Priority	8. TBV Due To		
	2. Technical Product Input Source Title and Identifier(s) with Version	3. Section					Unqual.	From Uncontrolled Source	Un-confirmed
2a 19	Sanders, T.L.; Seager, K.D.; Rashid, Y.R.; Barrett, P.R.; Malinauskas, A.P.; Einziger, R.E.; Jordan, H.; Duffey, T.A.; Sutherland, S.H.; and Reardon, P.C. 1992. *A Method for Determining the Spent-Fuel Contribution to Transport Cask Containment Requirements.* SAND90-2406. Albuquerque, New Mexico: Sandia National Laboratories. TIC: 232162.	page III-73	N/A Used as a reference only.	5.1, 5.2.5	normalized stress intensity factor for a surface crack in a tube subjected to bending loads	N/A	N/A	N/A	N/A
20	Roark, R.J. 1989. *Roark's Formulas for Stress and Strain, Sixth Edition.* New York, New York: McGraw-Hill Book Company. TIC: 10191.	page 67, item 15	N/A Data are established fact.	5.1, 5.3.1	equation for moment of inertia of a hollow circle	N/A	N/A	N/A	N/A
21	Roark, R.J. 1989. *Roark's Formulas for Stress and Strain, Sixth Edition.* New York, New York: McGraw-Hill Book Company. TIC: 10191.	page 96	N/A Data are established fact.	5.1, 5.3.1	equation for maximum fiber stress in a simple beam	N/A	N/A	N/A	N/A

OFFICE OF CIVILIAN RADIOACTIVE WASTE MANAGEMENT
DOCUMENT INPUT REFERENCE SHEET

1. Document Identifier No./Rev.:	Change:	Title:
CAL-EBS-MD-000001 REV 00	N/A	Breakage of Commercial Spent Nuclear Fuel Cladding by Mechanical Loading

Input Document			4. Input Status	5. Section Used in	6. Input Description	7. TBV/TBD Priority	8. TBV Due To		
	2. Technical Product Input Source Title and Identifier(s) with Version	3. Section					Unqual.	From Uncontrolled Source	Un-confirmed
2a 22	Roark, R.J. 1989. *Roark's Formulas for Stress and Strain, Sixth Edition.* New York, New York: McGraw-Hill Book Company. TIC: 10191.	page 101, item 1d	N/A Data are established fact.	5.1, 5.3.1	equation for maximum bending moment in a simple beam with left end fixed, right end fixed	N/A	N/A	N/A	N/A
23	Abramowitz, M. and Stegun, I.A., ed. 1972. "Handbook of Mathematical Functions with Formulas, Graphs, and Mathematical Tables." *National Bureau of Standards, Applied Mathematics Series 55.* Washington, D.C.: U.S. Department of Commerce. TIC: 229060.	page 69, item 4.2.1	N/A Data are established fact.	5.1, Att. III	equation for series expansion for exponential function	N/A	N/A	N/A	N/A
24	Lide, D.R., ed. 1995. *CRC Handbook of Chemistry and Physics, 76th Edition 1995-1996.* Boca Raton, Florida: CRC Press. TIC: 216194.	page 1-4	N/A Data are established fact.	5.1, 5.3.1	standard acceleration of gravity	N/A	N/A	N/A	N/A

OFFICE OF CIVILIAN RADIOACTIVE WASTE MANAGEMENT
DOCUMENT INPUT REFERENCE SHEET

1. Document Identifier No./Rev.:	Change:	Title:
CAL-EBS-MD-000001 REV 00	N/A	Breakage of Commercial Spent Nuclear Fuel Cladding by Mechanical Loading

Input Document							8. TBV Due To		
	2. Technical Product Input Source Title and Identifier(s) with Version	3. Section	4. Input Status	5. Section Used in	6. Input Description	7. TBV/TBD Priority	Unqual.	From Uncontrolled Source	Un-confirmed
2a 25	CRWMS M&O 1999. *Seismic Ground Motion Hazard Inputs.* Input Transmittal WP-NEP-99309.Ta. Las Vegas, Nevada: CRWMS M&O. ACC: MOL.19991019.0379. INITIAL USE	page A1-3 (item 1) page A1-5 (item 2)	TBV-3481	5.1, 5.2, 5.2.6, Att. V	(1) mean seismic hazard for horizontal peak ground velocity, (2) mean seismic hazard for vertical peak ground velocity	2	✓	N/A	N/A
26	CRWMS M&O 1999. *Seismic Ground Motion Hazard Inputs.* Input Transmittal WP-NEP-99309.Ta. Las Vegas, Nevada: CRWMS M&O. ACC: MOL.19991019.0379.	page A1-2 (item 1) page A1-4 (item 2)	N/A Used as a reference only.	5.2	(1) plot of mean seismic hazard for horizontal peak ground velocity, (2) plot of mean seismic hazard for vertical peak ground velocity	N/A	N/A	N/A	N/A
27	CRWMS M&O 1999. *Breakage of Commercial Spent Nuclear Fuel Cladding by Mechanical Loading.* TDP-EBS-MD-000001 REV 00. Las Vegas, Nevada: CRWMS M&O. ACC: MOL.19990722.0024.	entire	N/A Used as a reference only.	1	development plan for calculation	N/A	N/A	N/A	N/A